Titre: Title:	Repeatability and parasitic out-of-plane motion in controlled rocking structures with cylindrical columns: results from triaxial shake table tests
Auteurs: Authors:	Antonios Katsamakas
Date:	2026
Type:	Article de revue / Article
Référence: Citation:	Katsamakas, A. (2026). Repeatability and parasitic out-of-plane motion in controlled rocking structures with cylindrical columns: results from triaxial shake table tests. Earthquake Engineering & Structural Dynamics, 18 pages. https://doi.org/10.1002/eqe.70231

Earthquake Engineering & Structural Dynamics

WILEY

RESEARCH ARTICLE OPEN ACCESS

Repeatability and Parasitic Out-of-Plane Motion in Controlled Rocking Structures With Cylindrical Columns: Results From Triaxial Shake Table Tests

Antonios A. Katsamakas

Department of Civil, Geological and Mining Engineering, Polytechnique Montréal, Montreal, Canada

Received: 30 March 2026 | **Revised:** 1 June 2026 | **Accepted:** 10 June 2026

Keywords: controlled rocking | damage avoidance | parasitic out-of-plane motion | repeatability | self-centering | shake table testing

ABSTRACT

Self-centering rocking structures outperform conventional ones since they show zero post-earthquake damage and excellent recentering; however, their applications remain limited due to concerns that rocking is extremely sensitive and nonrepeatable. This paper investigates the repeatability and parasitic out-of-plane motion of controlled rocking structures with cylindrical columns through large-scale triaxial shake table tests. The specimen comprised four slender reinforced concrete columns restrained with unbonded steel tendons that provided positive post-uplift stiffness, representing a bridge-like structure at 1:5 scale. A total of 16 shake table tests were performed: five pairs of nominally identical triaxial tests to assess repeatability and six tests with varying directional excitation to quantify out-of-plane motion. The ground motions induced large displacements. Results show high repeatability of the shake table response. Displacements showed correlation coefficients of 0.85 for entire time histories. Maximum responses, which govern design, showed near-perfect repeatability with correlation coefficients of 0.90 and errors below 10%. No systematic relationship between response amplitude and repeatability was observed. Under planar (one-directional) seismic excitation, parasitic out-of-plane motion was low compared to uncontrolled rocking systems, with average out-of-plane to in-plane displacement ratios below 25%. Independent planar analyses, when geometrically combined, can estimate the bidirectional response with reasonable accuracy. The results contradict the perception that rocking behavior is nonrepeatable and show that controlled rocking structures with inherent frictional and impact damping can exhibit repeatable seismic response even without supplemental energy dissipation.

1 | Introduction

Rocking structures uplift from their base when subjected to strong ground shaking. Rocking is inherent in the seismic response of a wide range of non-engineered structures [1], including columns of ancient temples [2–4] and the out-of-plane response of masonry [5–18]. Moreover, rocking is prevalent in the seismic response of slender, freestanding structural components [19–33]. After uplift, a conventional (uncontrolled/unenhanced) rocking oscillator has negative stiffness; hence, its behavior cannot be related to any equivalent elastic system [34].

Over the last decades, rocking isolation has emerged as a seismic design strategy where self-centering structures are intentionally designed to uplift and rock during strong earthquakes. These structures can be more resilient, economical, and sustainable than conventional structures designed according to capacity design. To improve performance, rocking structures can be coupled with supplemental restrainers (additional stiffness) and energy dissipation devices (additional damping), resulting in *controlled* rocking systems. Self-centering structures outperform conventional ones by exhibiting zero or minimal post-earthquake damage and negligible residual displacements. This not only ensures life safety but also allows immediate occupancy after major seismic events without extensive repairs. The reduced need for post-earthquake repairs improves economic competitiveness. Moreover, self-centering structures can use less material and achieve lower costs and environmental impact, as the isolation effect of rocking allows structural members and foundations to be designed for significantly lower seismic loads [35].

The principles of rocking isolation are applicable to bridges [36–51], buildings [52–58], and other structures across different materials, including concrete, steel, and timber [59–68]. Since rocking structures are modular rather than monolithic, their structural members can be prefabricated, reducing construction time and improving quality control. Their modular nature also makes them adaptable and reconfigurable, enabling nondestructive decommissioning, repair, and reuse of structural members at the end of their service life.

Despite their numerous advantages, real-world applications of rocking structures remain extremely limited [69]. One of the main reasons is the widespread perception that rocking is extremely sensitive, hence nonrepeatable and unpredictable [70]. Sensitivity, repeatability, and predictability are intertwined and often used interchangeably, so their meaning in this study is clarified below:

- *Sensitivity*: A system is sensitive to the parameters that define it (e.g., geometry, initial conditions, seismic motion) when a small perturbation of these parameters leads to a significantly different seismic response. The earthquake engineering community has loosely used the term "chaotic" to describe such systems [71].
- *Repeatability*: When the same structure is subjected to the same ground motion in two sequential, nominally identical shake table tests, the response should be identical. However, even under well-controlled laboratory conditions, two sequential tests cannot be perfectly identical. Hence, a very sensitive ("chaotic") structure exhibits a nonrepeatable response in these repeatability tests, since the minor (unavoidable) differences between the tests become crucial.
- *Predictability*: The seismic response of a structure is predictable when numerical models can capture its shake table response. A nonrepeatable system cannot be predictable in a deterministic sense; when tests are nonrepeatable, no experimental test can serve as a benchmark.

Uncontrolled (unenhanced) rocking structures are indeed very sensitive to their parameters. The seminal study of Yim et al. [70] proved that small changes in geometry or ground motion input lead to significantly different earthquake responses, and nonrepeatable shake table tests. Aslam et al. [72] showed that a small change in the coefficient of restitution significantly alters the seismic response of rocking blocks. Lachanas and Vamvatsikos [73] and Lachanas et al. [74] showed that, in the deterministic sense, uncontrolled rocking block oscillations are extremely sensitive to the vertical component of the excitation. Drosos and Anastasopoulos [75] observed that multidrum rocking columns have significantly different residual displacements when subjected to identical shake table tests. Vassiliou et al. [76] observed nonrepeatable shake table results when testing uncontrolled cylindrical columns.

To overcome the sensitivity of uncontrolled rocking structures to a single ground motion, previous studies proposed using the cumulative distribution function (CDF) to describe the statistical response of structures to a group of ground motions [77–88]. This method is statistically accurate and compatible with the stochastic nature of seismic design. When designing a structure, one uses a group of ground motions that define the seismic hazard of the given location, and the question becomes the statistical response of the structure to this group of ground motions (not the response to a single ground motion). Moreover, CDF curves are a powerful visualization tool that allows the identification of trends in large datasets. However, this method has reasonable limitations: (i) it is time-consuming and requires significant computational resources (as it requires numerous time-history analyses), and (ii) the selection of the number and properties of the ground motions used is nontrivial, as no such guidelines exist [89].

In contrast to *uncontrolled* rocking structures, numerous studies on *controlled* rocking structures have shown repeatable and predictable results. Zaki et al. [89] provide a detailed review on this topic, which is briefly summarized here for completeness. Midorikawa et al. [90] tested a controlled rocking concentrically braced frame (CBF) with yielding base plates at its base. The rocking rotations were limited to 0.01α (where α is the slenderness of the rocking block) and showed good agreement with numerical models. Tremblay et al. [35] and Mottier et al. [91] tested two-story controlled rocking CBFs with external dampers to rocking rotations up to 0.04α. The numerical models predicted the roof displacement well. Wiebe and Christopoulos [92–94] and Wiebe et al. [95, 96] tested eight-story controlled rocking CBFs with auxiliary post-tensioning, friction devices, and a second rocking joint at the frame's mid-height to limit higher mode effects. As before, the numerical and experimental results were in good agreement.

Zaki et al. [89] used planar analytical models to assess the sensitivity of rocking structures with varying levels of auxiliary stiffness, damping, and superstructure properties. They compared the maximum displacement of benchmark rocking systems with that of the same systems subjected to a $\pm 10\%$ perturbation in either the column height, slenderness ratio, or coefficient of restitution. They also evaluated the effectiveness of auxiliary stiffness, auxiliary damping, and superstructure characteristics in reducing system sensitivity. The sensitivity of the rocking systems was then compared to that of conventional elastoplastic systems. Their results indicated that by adding supplemental damping, increasing the contribution of superstructure, and limiting rocking rotation below 0.05α, the sensitivity of rocking systems to perturbations can be substantially reduced and become comparable to that of conventional elastoplastic systems. Although the authors noted that experimental studies are required to validate these analytical findings, the results provide valuable insights for understanding the fundamental aspects of sensitivity, repeatability, and predictability in rocking structures, which currently constrain their practical application.

All the aforementioned experimental studies on controlled rocking structures share the following characteristics:

i) Very low rocking rotations (below 0.05α): This means that the displacements were below 5% of the static displacement that would topple the uncontrolled rocking block. Under strong earthquakes, maintaining low displacements requires high auxiliary stiffness through stiff supplemental restrainers (tendons). This leads to high forces in the superstructure and requires adequately strong structural members. As an alternative design approach, allowing larger displacements could lead to improved seismic isolation effects.

ii) External damping enhancements: The studies use yielding plates/rebars, friction damping, or viscous damping to limit displacements. Despite the undeniable efficiency of these methods, many have argued that rocking structures inherently have considerable damping (due to impact and friction); with some even claiming that this inherent damping suffices to ensure very high seismic stability [97].

iii) Consideration of only planar response: The consideration of planar response is a necessary and valuable first step; however, a lack of sensitivity in the planar rocking response does not guarantee the same in the three-dimensional (3D) rocking response, which is known to be much more complicated [76, 77]. Moreover, the sensitivity of cylindrical rocking columns has not been studied. Cylindrical rocking columns have been widely used since antiquity and have inherently coupled 3D response; since their base is circular, planar excitation leads to 3D rocking/wobbling and "parasitic" displacements in the out-of-plane direction. In fact, in shake table tests of uncontrolled cylindrical rocking columns [75], "parasitic" out-of-plane motion was oftentimes larger than the in-plane motion.

Following the valuable recent findings of [89] on the sensitivity of rocking and the limitations identified in the existing literature, the present study investigates the repeatability and parasitic out-of-plane motion in controlled rocking structures with cylindrical columns through large-scale shake table tests. This study is the first to investigate the repeatability of controlled rocking structures with positive post-uplift stiffness: (i) under large displacements (rotations); (ii) with cylindrical columns; (iii) without additional damping; (iv) under triaxial seismic excitation. Moreover, it is the first study to investigate the parasitic out-of-plane motion of controlled rocking structures with cylindrical columns.

This paper provides experimental results on the long-standing discussion about the sensitivity, repeatability, and predictability of rocking motion, including the role of inherent damping (impact and friction). The results aim to facilitate the design and implementation of controlled rocking structures with positive post-uplift stiffness. Moreover, the paper quantifies the parasitic out-of-plane motion in controlled rocking structures with cylindrical columns, assesses the accuracy of performing independent planar analyses for two horizontal directions and combining the results, and facilitates the design and execution of shake table tests of such structures using uniaxial shake tables (which are much more common than two- or three-directional ones).

2 | Mechanics of the Controlled Rocking Frame

The lateral force–displacement relation of a controlled rocking frame with unbonded tendons (anchored at the bottom end of the columns and at the top of the slab) appears in Equation (1).

$$F = [(0.5+\gamma) N m_c g \alpha \operatorname{sgn}(u)] + [0.5 N k_{res} b\alpha - (0.5+\gamma) N m_c g] \frac{u}{2h} \tag{1}$$

In Equation (1) and Figure 1, m_c is the mass of each column, m_b is the mass of the cap beam (slab), and N is the total number of columns. The slab-to-column mass ratio is defined as $\gamma = m_b/(N \times m_c)$. The diameter and height of the column are $2b$ and $2h$, respectively. The semi-diagonal of the column, its slenderness, and its tilt angle are R, $\alpha = 2b/2h$, and θ, respectively. The gravitational acceleration is g. Under lateral force F, the lateral displacement of the frame is u. The axial stiffness of the tendons is k_{res}. The "critical" value of the tendon stiffness is noted as k_{crit}, with $k_{res} > k_{crit}$, $k_{res} = k_{crit}$, and $k_{res} < k_{crit}$ leading to positive, zero, and negative post-uplift stiffness, respectively [98, 99]. From Equation (1), it follows that $k_{crit} = \frac{[(1+2\gamma)m_c g]}{\alpha b}$. The post-uplift stiffness of the frame is given in Equation (2):

$$K_{post-uplift} = \left[\frac{1}{2} N k_{res} b\alpha - \left(\frac{1}{2}+\gamma\right) N m_c g\right] \frac{1}{2h} \tag{2}$$

When $K_{post\text{-}uplift}$ is positive and by lumping half of the column mass at the top and half at the bottom, the structural eigenperiod is calculated using Equation (3):

$$T_{post-uplift} = 2\pi\sqrt{\frac{m_b + (0.5 N m_c)}{K}} \tag{3}$$

Figure 1C plots the "pushover" response of the controlled rocking frame for increasing values of k_{res}. For negative post-uplift stiffness systems, the "displacement capacity" is the point of neutral equilibrium (overturn) [99]. For $k_{res} = 0$ (no tendons), the displacement capacity of the frame equals the base of the column ($2b$). The displacement capacity increases with increasing k_{res}. The post-uplift stiffness is zero for $k_{res} = k_{crit}$. When $k_{res} > k_{crit}$, the post-uplift stiffness becomes positive, and the displacement capacity of the system is no longer related to overturning; failure is only governed by tensile fracture of the tendons or material failure of the columns. Anchoring the tendon within the foundation would increase the post-uplift stiffness of the restraining system by a factor of four [99].

3 | Shake Table Testing

3.1 | Specimen Description

The specimen comprised four columns and a slab (Figure 2). This specimen was tested in Ref. [97] under 184 triaxial design-level ground motions and showed zero damage and minimal residual displacements. As it is highly resilient, it is used in the present paper to investigate in detail two additional and independent phenomena: repeatability and parasitic out-of-plane motion. The prototype-to-model scale was $S_L = 1/5$. The scaling laws for reduced-scale physical modeling appear in Ref. [100]. To preserve similitude, the ground motions were scaled in frequency

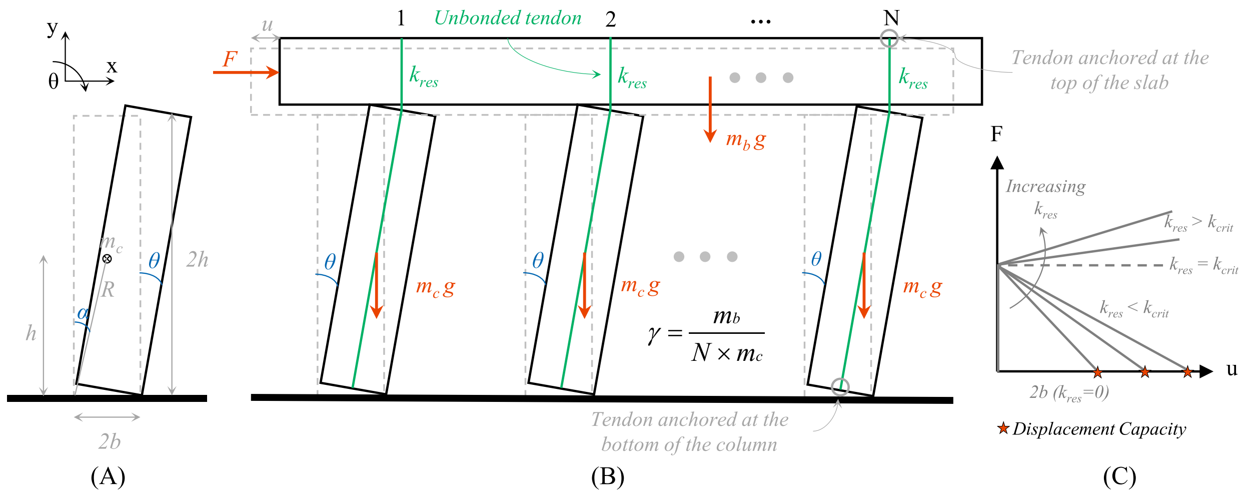

FIGURE 1 | (A) Sketch of a freestanding rocking block; (B) sketch of a controlled rocking frame; (C) lateral force–displacement response of the frame for varying $k_{res.}$

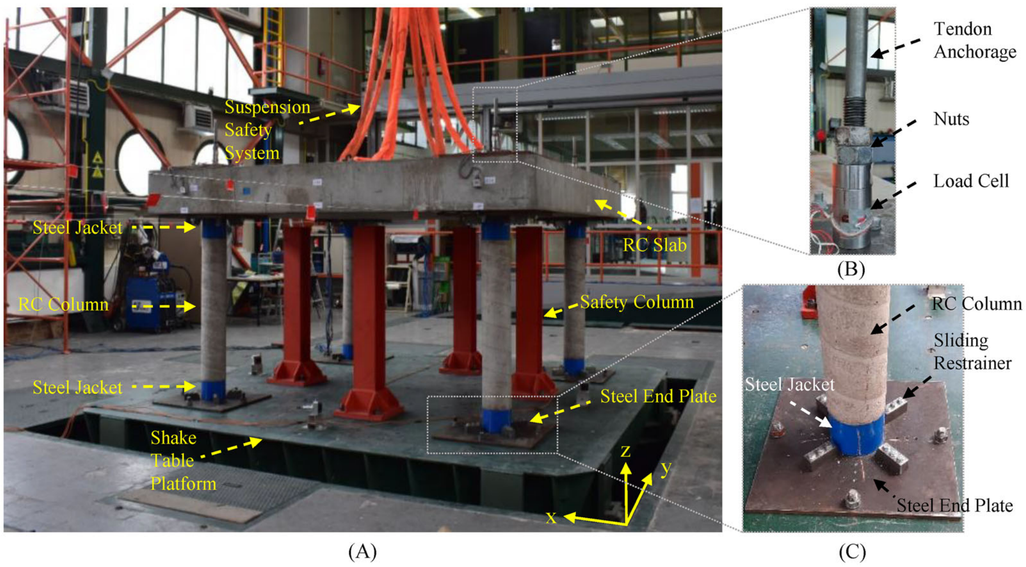

FIGURE 2 | (A) View of the controlled rocking specimen; (B) detail of the top anchorage of the tendon; (C) detail of the base of the freestanding piers and the sliding restrainers.

by $\sqrt{5}$ so that the model represents a prototype with five times larger columns. All elements were made of reinforced concrete (RC). The total mass of the slab and the four columns was approximately 9435 and 550 kg, respectively, leading to a slab-to-column mass ratio of $\gamma = 17$. An unbonded (ungrouted) steel tendon passes through each column. It is anchored at the base of the columns (through a socket clamped on the tendon and a threaded tube welded at the bottom of the steel jacket) and above the slab (using a similar connection) (Figure 3B,C,E). The specimen is a simplified model of a bridge, and its dimensions appear in Figure 3. The construction details can be found in [101]. The slab weight results in a normalized axial load in the columns equal to $\nu = N/(A_c \times f_{cd}) = 3.3\%$, where N is the axial load, A_c is the cross-sectional area of the column, and f_{cd} is the design compressive strength of concrete. This value is on the low side of realistic values in bridge design. The specimen was symmetric without deliberate mass eccentricity; future studies are encouraged to study this effect. Moreover, even under controlled laboratory conditions, specimens have minor imperfections that break symmetry and induce torsion. Practical applications must account for these deviations.

Steel plates were welded on the top of the columns to restrain lateral motion of the tendon within its duct. The tendon was a 19-wire strand with an external diameter of 16 mm. The wires were placed in a 12 × 6 × 1 configuration (Figure 3D). Three tendons were tested in uniaxial tension to obtain their mechanical properties. The average strength and stiffness of the tendons were 160.3 kN and 7200 kN/m, respectively. According to Equation (3), this gives a post-uplift eigenperiod of 2.2 s in the model scale (4.9 s in the prototype scale). For seismic isolation applications, this eigenperiod is quite high, but recentering is guaranteed in rocking

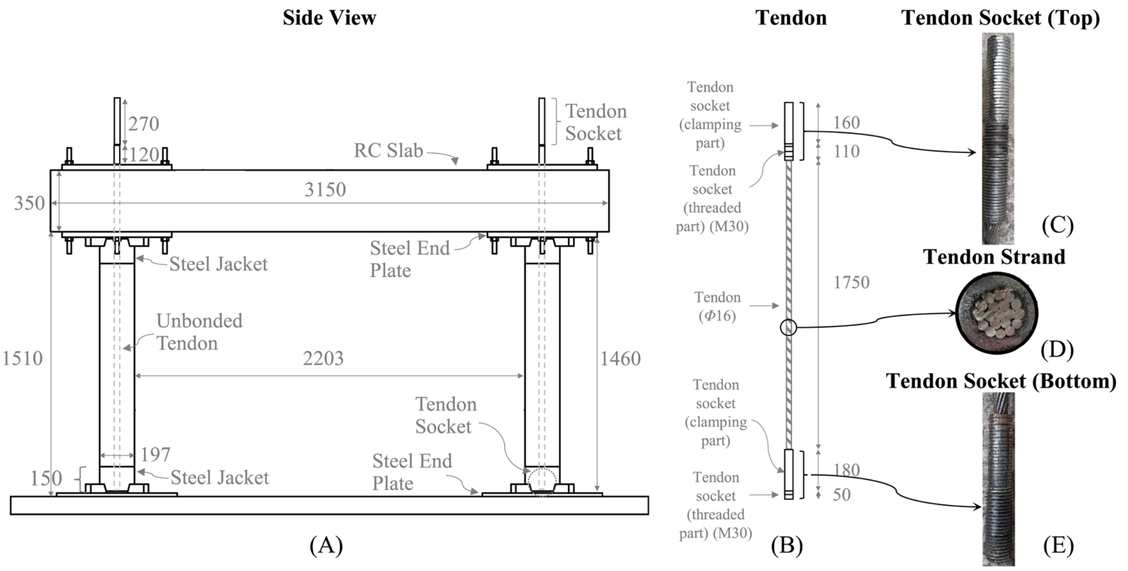

FIGURE 3 | (A) Side view of the controlled rocking specimen; (B) unbonded tendon; (C) detail of the top tendon socket; (D) detail of the tendon strand; (E) detail of the bottom tendon socket. All dimensions are in millimeter.

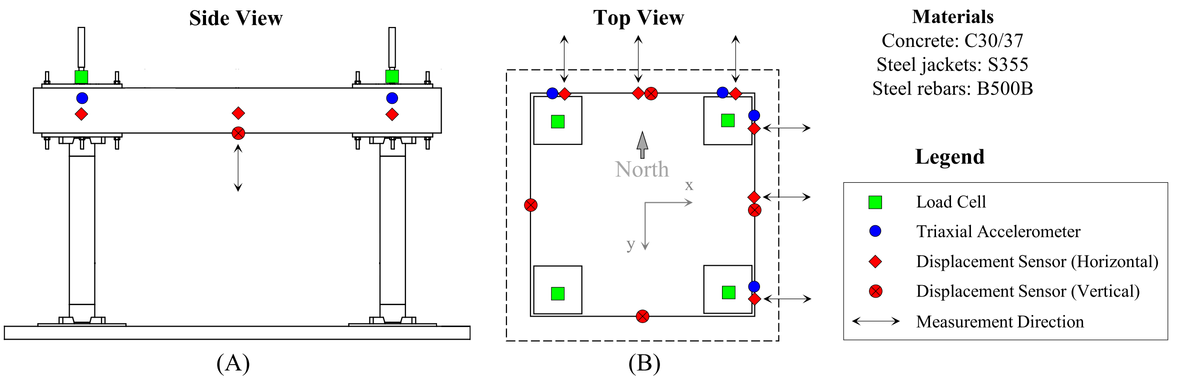

FIGURE 4 | Instrumentation of the shake-table tests. (A) Side view; (B) top view.

systems even at such long isolation periods. The structure did not comprise external energy dissipaters.

3.2 | Shake Table Specifications

The shake table tests were performed at the Laboratory for Earthquake Engineering (LEE) of the National Technical University of Athens (NTUA). The shake table comprises a 4×4 m, six-degrees-of-freedom platform. The displacement and velocity capacities of the shake table are ±100 mm and 1000 mm/s, respectively. Under a maximum payload of 10 tons, the shake table can apply accelerations of 2 and 4 g in the two horizontal and vertical directions, respectively.

3.3 | Instrumentation

The RC slab was instrumented with four triaxial accelerometers (Figure 4). The horizontal displacements of the slab, from which the slab rotation was computed, were measured using 6 draw-wire displacement sensors. Three of these sensors were placed in the northern part of the RC slab to measure displacements parallel to the y-axis, and the remaining three were placed in the eastern part to measure displacements parallel to the x-axis (Figure 4). Four cable-extension position transducers, located at the center of each side of the RC slab, measured the vertical displacements (Figure 4). All displacements were recorded using cable-extension position transducers with an accuracy of 0.1%. All tendons were equipped with uniaxial load cells at their top ends (Figures 2B and 4). Eight additional accelerometers and displacement sensors integrated into the shake table actuators measured the acceleration and displacement of the shake table. The accelerations were recorded with an accuracy of 0.01% of the measured value. The sampling frequency of all measurements ranged between 225 and 450 Hz, depending on the duration of the ground motion.

3.4 | Response Quantities of Interest

The main response quantities extracted from the experimental data were as follows:

TABLE 1 | List of the ground motions used.

Test no.	Test type	*M*	Year	Name	Recording station	PEER RSN	Type	Component
1–2	Repeatability	7.5	1999	Kocaeli	Duzce	1158	FF	X, Y, Z
3–4	Repeatability	6	1987	Whittier Narrows-01	Downey—Birchdale	614	FF	X, Y, Z
5–6	Repeatability	7	2010	El Mayor–Cucapah	El Centro Array #12	8161	NFP	X, Y, Z
7–8	Repeatability	6.5	1987	Superstition Hills-02	Parachute Test Site	723	NFP	X, Y, Z
9–10	Repeatability	6.5	1979	Imperial Valley-06	Bonds Corner	160	NFNP	X, Y, Z
11	Parasitic out-of-plane	6.4	1983	Coalinga-01	Parkfield—Fault Zone 14	338	FF	X
12	Parasitic out-of-plane	6.4	1983	Coalinga-01	Parkfield—Fault Zone 14	338	FF	Y
13	Parasitic out-of-plane	6.4	1983	Coalinga-01	Parkfield—Fault Zone 14	338	FF	X, Y
14	Parasitic out-of-plane	7.3	1992	Landers	Coolwater	848	FF	X
15	Parasitic out-of-plane	7.3	1992	Landers	Coolwater	848	FF	Y
16	Parasitic out-of-plane	7.3	1992	Landers	Coolwater	848	FF	X, Y

i. The displacement at the center of the slab (relative to the shake table) along the x- and the y-axis, (Displ.X, Displ.Y), as well as its norm, equal to:

$$\text{Displ.} = \sqrt{(\text{Displ.}\ X)^2 + (\text{Displ.}\ Y)^2}\,.$$

ii. The slab rotation (torsion) around its vertical axis (z-axis). The slab rotation around the x- or the y-axis was negligible.

iii. The tendon forces (TF) of the four tendons.

iv. The acceleration at the center of the slab along the x- and the y-axis, (A_X, A_Y), as well as its norm equal to

$$\text{Accel.} = \sqrt{(\text{Accel.}\ X)^2 + (\text{Accel.}\ Y)^2}\,.$$

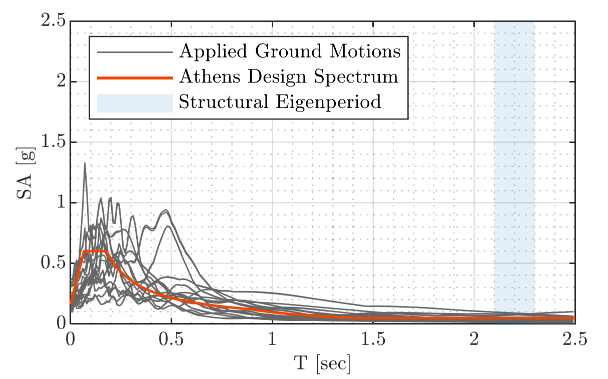

FIGURE 5 | Pseudo-acceleration elastic response spectra ($\zeta = 5\%$) of the ground motions used in the shake table tests and comparison with the design spectrum of Athens, Greece.

3.5 | Ground Motion Selection

A total of 16 shake table tests were performed within the framework of the present study. The ground motions originated from all three categories of FEMA P695 [102], including near-field pulse-like (NFP), near-field no pulse-like (NFNP), and far-field (FF). As the tests were conducted at 1:5 scale (length scale $S_L = 1/5$), the ground motions were time-scaled to $S_T = \sqrt{S_L} = 0.447$. Table 1 lists the ground motions used, whereas Figure 5 plots the elastic spectra ($\zeta = 5\%$) of the as-applied ground motions, together with the design spectrum of Athens, Greece, according to EC8 [103], assuming soil type A and importance factor 1, also scaled in time by 0.447. The blue-shaded area of Figure 5 shows the range of the structural eigenperiod, which ranges between $T = 2.1$ s and $T = 2.3$ s, depending on the definition of the tendon stiffness (secant stiffness at different load levels) and using Equation (2). In prototype scale, the eigenperiod ranged between $T = 4.7$ s and $T = 5.1$ s.

3.6 | Repeatability Assessment

Conventional (monolithic) bridges are severely damaged after design-level ground motions. This makes repeatability tests impossible, as the same structure cannot be tested twice. However, rocking bridges show minimal or zero damage and residual displacements under design-level earthquakes; thus, repeatability tests are possible. Tests 1–10 assessed the repeatability of the shake table response. These tests were organized in five identical pairs: Tests 1–2, 3–4, 5–6, 7–8, and 9–10 (i.e., Test 2 replicated Test 1, Test 4 replicated Test 3, etc.). Tests 1–10 were triaxial, meaning that all three components of ground motion (X, Y, Z) were applied simultaneously (Table 1). After each test, the structure was inspected for damage. Since no damage was observed, the structure was tested again. It should be noted that two sequential nominally identical shake table tests are never fully identical due to inherent perturbations between tests. These perturbations originate from the following two sources:

i) Signal reproduction error: The applied motion inevitably differs from the target motion due to inherent system nonlinearities and dynamic interactions between the table and the specimen. This discrepancy is nonconstant; consequently, the applied motions are never identical across repeated tests [104].

ii) Imperfect recentering: After each test, the specimen did not return exactly to its initial position. The residual displacements were minimal (a few millimeters), yet nonzero. Since the residual displacements were so small, manual recentering would not improve accuracy and was not performed. As a result, the initial position between nominally identical tests differed.

3.7 | Parasitic Out-of-Plane Motion Assessment

Rocking structures with cylindrical columns are known to exhibit significant out-of-plane response when subjected to planar excitation due to wobbling. Tests 11–16 were performed to assess this parasitic out-of-plane motion. Depending on the test, specific components of the ground motion were applied (X only, Y only, or X and Y simultaneously), as seen in Table 1. For example, Test 11 applied only the X component of the Coalinga-01 ground motion, Test 12 applied only the Y component of the same ground motion, and Test 13 applied both the X and Y components simultaneously. The same procedure was followed for Tests 14–16. The objectives were (i) to assess the magnitude of the out-of-plane response when the excitation is planar, and (ii) to evaluate whether applying each component independently in different tests and combining the results would yield the same outcome as applying both components simultaneously in one test.

3.8 | Quantification Metrics

To quantify the repeatability and the parasitic out-of-plane motion of the shake table tests, the following metrics are used [105]:

- Pearson correlation coefficient (R): R quantifies the linear similarity between data points (or time histories). It ranges between $R = -1$ and $R = 1$. $R = 1$ and $R = -1$ indicate perfect positive or perfect negative linear correlation. $R = 0$ indicates zero correlation.
- Normalized mean absolute error (NMAE): The NMAE quantifies the average pointwise discrepancy between two time histories, normalized by the characteristic amplitude of the reference signal and expressed as a percentage, with lower values indicating lower error and higher correlation. For example, an NMAE of 10% indicates that the average absolute difference between the two time histories equals 10% of the characteristic amplitude.
- Root-Mean-Square (RMS) ratio (C_{rms}): C_{rms} quantifies the relative amplitude of two time histories by comparing their RMS values. C_{rms} is expressed as a percentage. For example, $C_{rms} = 10\%$ indicates that the out-of-plane response is, on average, 10% of the in-plane response.
- Energy-based coupling index (C_{energy}): C_{energy} quantifies the cumulative out-of-plane response energy relative to the in-plane response energy over the entire record duration, based on the time-integrated squared response histories. It shows the relative distribution of response energy between the two directions. The term "energy" refers here to the time-integrated squared response (signal energy) and not to the physical mechanical energy of the structure. For example, $C_{energy} = 10\%$ means that the out-of-plane energy is 10% of the in-plane. C_{energy} can exceed 100%, which would mean that the out-of-plane response is larger than the in-plane response.

4 | Results

4.1 | Repeatability Results

Figures 6 and 7 provide detailed insights into the repeatability of the shake table response. Figure 6 shows the repeatability results of the tests with the lowest response (Tests 3–4), where the maximum displacement was 16.5 mm ($\theta = 0.084\alpha$). Figure 7 shows the corresponding results for the tests with the largest response (Tests 9–10), where the maximum displacement was 74.8 mm ($\theta = 0.38\alpha$). Both figures show displacements along each horizontal axis (Disp.X and Disp.Y) and their resultant (Disp.), accelerations along each horizontal axis (Accel.X and Accel.Y) and their resultant (Accel.), slab rotation around its vertical axis, the tendon force of each tendon (TF), displacement orbits, and acceleration–displacement loops along each horizontal axis. The two lines (black and red) correspond to the two tests in each pair (Tests 3 and 4 or Tests 9 and 10, respectively). The correlation coefficient (R) and NMAE of the entire time history are noted inside each subplot.

The main conclusions from Figures 6 and 7 are summarized as follows:

- Displacements show high repeatability. The entire time history is largely identical and often indistinguishable, with $R = 0.74$–0.94 and NMAE = 5%–8%. The maximum displacements mostly appear at the same time instant and show very low errors (between 1% and 9%).

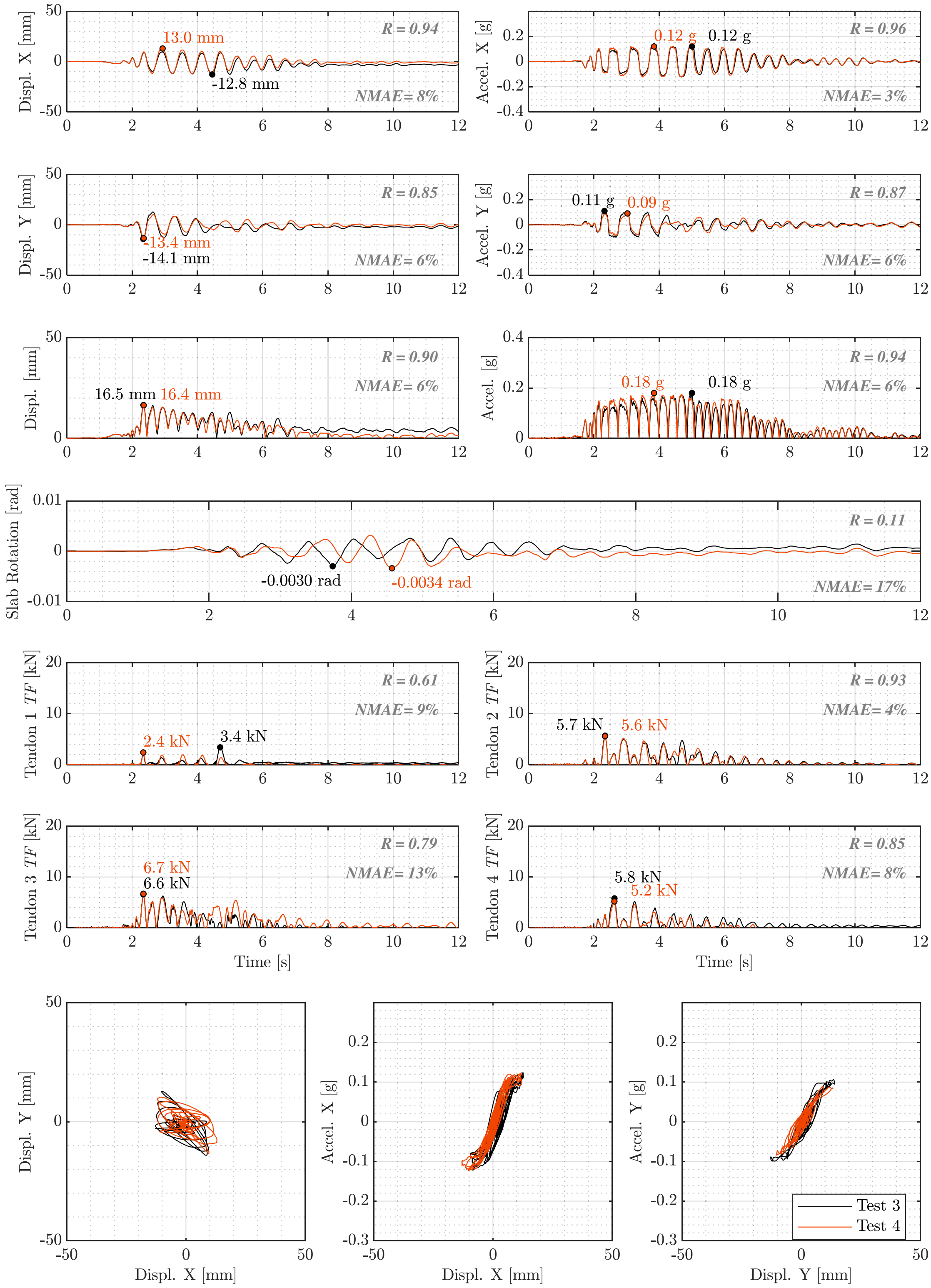

FIGURE 6 | Repeatability test and comparison of Tests 3 and 4.

- Accelerations are also repeatable, with R = 0.50–0.96, and NMAE = 3%–15%. The peak accelerations have negligible magnitude errors.
- Slab rotation clearly shows the lowest correlation, with R = 0.11–0.13 and NMAE = 17%–20%. This indicates high sensitivity of the rotational kinematics to small variations in boundary conditions. This phenomenon likely originates from the structure's rotational stiffness, which is arguably lower than its translational stiffness
- Tendon forces show moderate to high repeatability, with R = 0.61–0.93 and NMAE = 4%–13%. The average maximum force error was 6%. It is noted that, in theory, the tendon forces

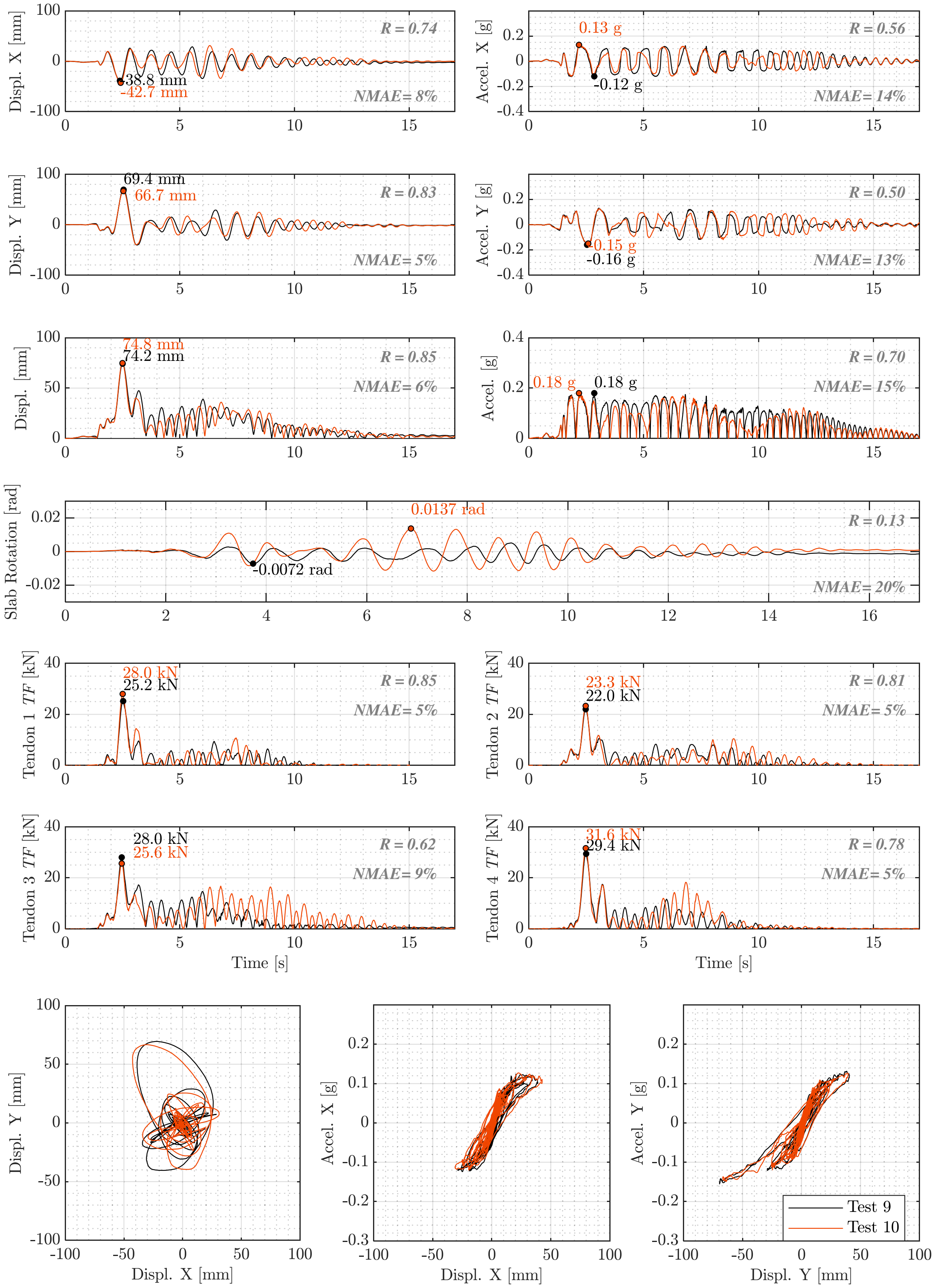

FIGURE 7 | Repeatability test and comparison of Tests 9 and 10.

should be identical for all four tendons. This is not observed because torsion and minor structural imperfections lead to asymmetric engagement of the tendons and varying forces among them.

- Displacement orbits and acceleration–displacement loops show consistent and repeatable patterns. The repeatable thickness of the acceleration–displacement loops indicates repeatable energy dissipation. In Figure 6, the structure

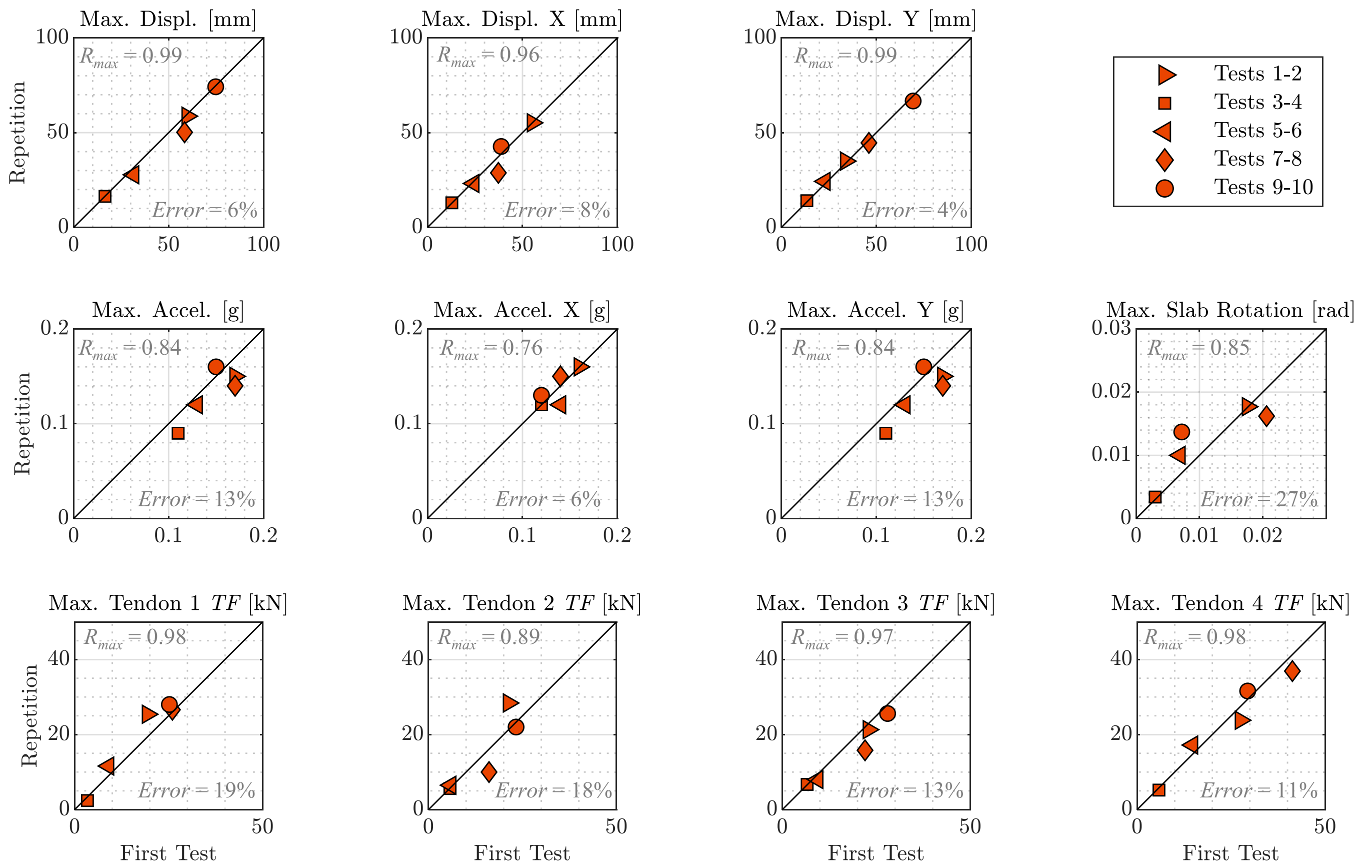

FIGURE 8 | Peak value of each response magnitude in the repeatability tests.

mainly remains in the pre-uplift phase, whereas in Figure 7, the structure enters the post-uplift phase.

Figure 8 shows the maximum response of each test (Tests 1–10) and its repetition in the form of scatter plots. The horizontal axis shows the maximum response of the first test (Tests 1, 3, 5, 7, and 9), whereas the vertical axis shows the corresponding magnitude for the repetition test (Tests 2, 4, 6, 8, and 10). Each subplot refers to a different response magnitude, as seen in the corresponding title. The correlation coefficient of the maximum responses (R_{max}) is noted inside each subplot, together with the average error between the tests. The different tests are indicated with different markers, as shown in the legend. The tests discussed in detail in Figures 6 and 7 are indicated with a red square (Tests 3–4) and a red circle (Tests 9–10). The conclusions from Figure 8 are summarized as follows:

- The results demonstrate high overall repeatability of the peak response for all metrics (R_{max} = 0.76–0.99).
- Maximum displacements show the highest repeatability, with near-perfect correlation (R_{max} = 0.96–0.99), followed by tendon forces (R_{max} = 0.89–0.98). Peak accelerations and rotations have the lowest correlation (R_{max} = 0.76–0.85), which is still high.
- Maximum displacements have the lowest error (4%–8%), followed by accelerations and tendon forces with errors of 6–13% and 11–19%, respectively. Slab rotations have the highest error with 27%.
- Tendon 4 has slightly higher tendon forces than the other three, but no systematic trend appears, with different tests leading to higher forces in different tendons.
- No systematic bias is observed, since the points are distributed both below and above the diagonal.
- The amplitude of the response does not systematically affect the repeatability. This means that small- and large- amplitude tests are equally repeatable.

To better understand the repeatability of the response, the correlation coefficient (R) of the entire time history (not of its peak value) appears on the vertical axis of Figure 9. The horizontal axis shows the maximum displacement of each pair of tests in an effort to identify trends between R and the response amplitude. The average R of the five test pairs (R_{mean}) is shown with a horizontal red dot-dash line. The R of the maxima (R_{max} from Figure 8) is shown with a black dashed line. The conclusions from Figure 9 are summarized as follows:

- Displacements consistently show the highest values of R, with limited scatter around R_{mean} = 0.8–0.89. Tendon forces are the second-most repeatable quantity, with R_{mean} = 0.75–0.84, followed by accelerations with R_{mean} = 0.68–0.77.
- Rotations are clearly the least repeatable quantity, with R_{mean} = 0.45 and high scatter of the points ranging from R = 0.11–0.82.

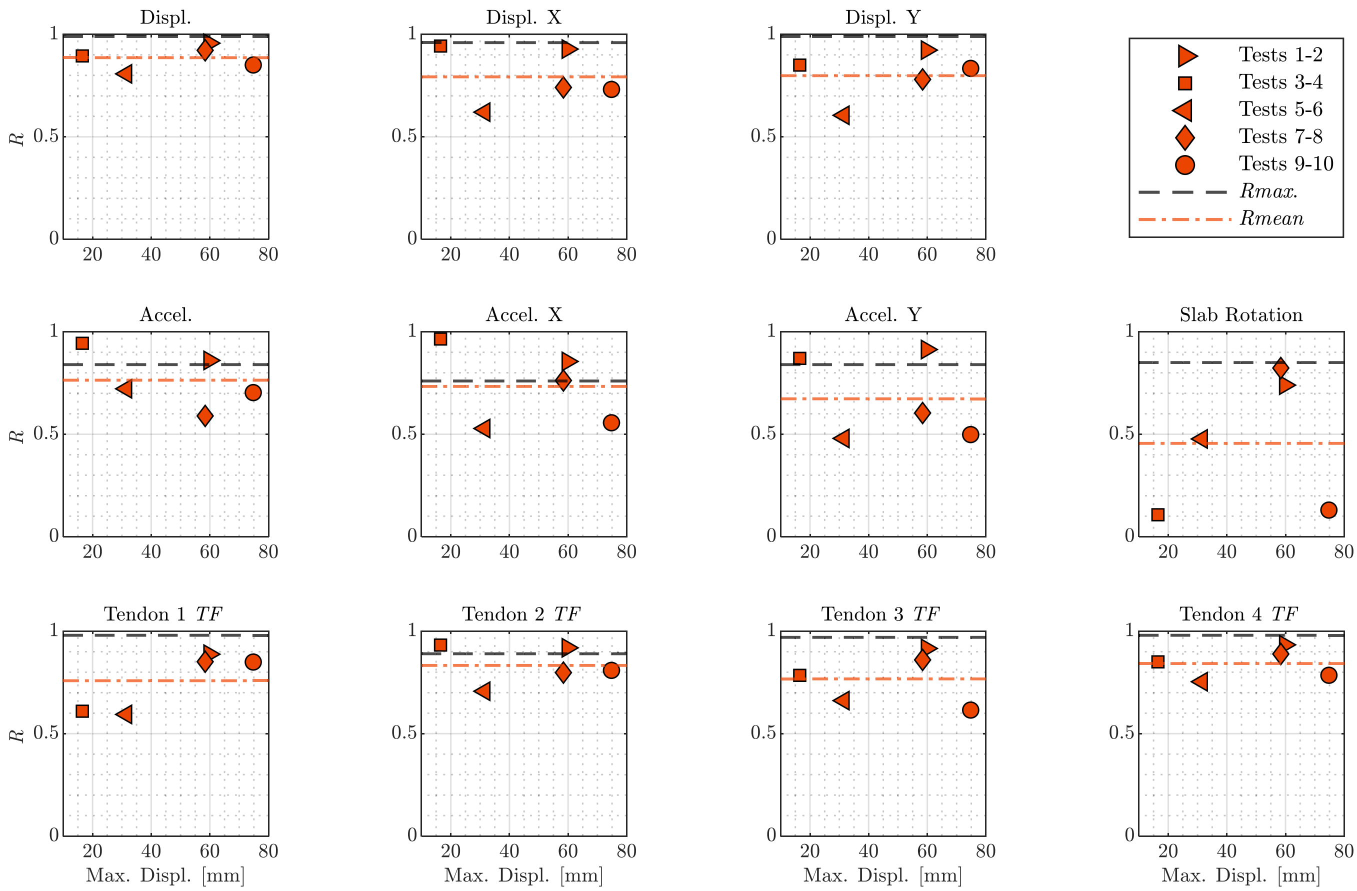

FIGURE 9 | Correlation coefficient (R) of the entire time history of each test and its repetition plotted against the maximum displacement of each test pair.

- As in R_{max}, no systematic trend is observed between R_{mean} and the amplitude of the response.
- In all cases, the R_{max} (dashed black line) is significantly higher than the average R of the entire time history, proving that the maximum response is much more repeatable than the entire time history. This is noteworthy, as the maximum response governs design.

The repeatability of the time history response was also quantified with the NMAE, which appears on the vertical axis of Figure 10. The horizontal axis shows the maximum displacement of each pair of tests to identify trends between NMAE and the response amplitude. The mean value of the five test pairs in each subplot appears as a dot-dash line ($NMAE_{mean}$). The conclusions from Figure 10 are summarized as follows:

- Overall, the response is repeatable with reasonable values of NMAE, and in most cases $NMAE_{mean} \leq 10\%$.
- Displacements consistently have the lowest error (NMAE $\leq$ 10%, $NMAE_{mean} \leq 6\%$), followed by tendon forces (NMAE $\leq$ 15%, $NMAE_{mean} \leq 8\%$) and accelerations (NMAE $\leq$ 20%, $NMAE_{mean} \approx 10\%$).
- Rotations have overall the highest error values and the highest scatter around those values (NMAE $\leq$ 21%, $NMAE_{mean} \approx 11\%$). This agrees with the conclusions from the previous metrics.
- No systematic correlation is observed between the amplitude of the response and NMAE. This agrees with the conclusions from the previous metrics.

4.2 | Out-of-plane

Figures 11 and 12 provide insights into the parasitic out-of-plane motion of controlled rocking structures (Tests 12 and 14). In these tests, only one horizontal excitation component is applied (components Y and X in Tests 12 and 14, respectively). Tests 12 and 14 are shown since they exhibit the largest and smallest out-of-plane response, respectively. The in-plane and out-of-plane responses are quantified using displacements, rotations, and accelerations. The conclusions from Figures 11 and 12 are summarized as follows:

- The out-of-plane response is generally small and much more limited than in the case of unrestrained rocking structures [75]. Significant uplift is observed in the in-plane response; however, the out-of-plane response remains in the pre-uplift range (Figures 11 and 12, bottom right).
- The ratio of the out-of-plane to in-plane maximum displacement is 9 mm/30.2 mm = 30% and 5.2 mm/29.8 mm = 17% for Tests 12 and 14, respectively (Figures 11 and 12, top left).

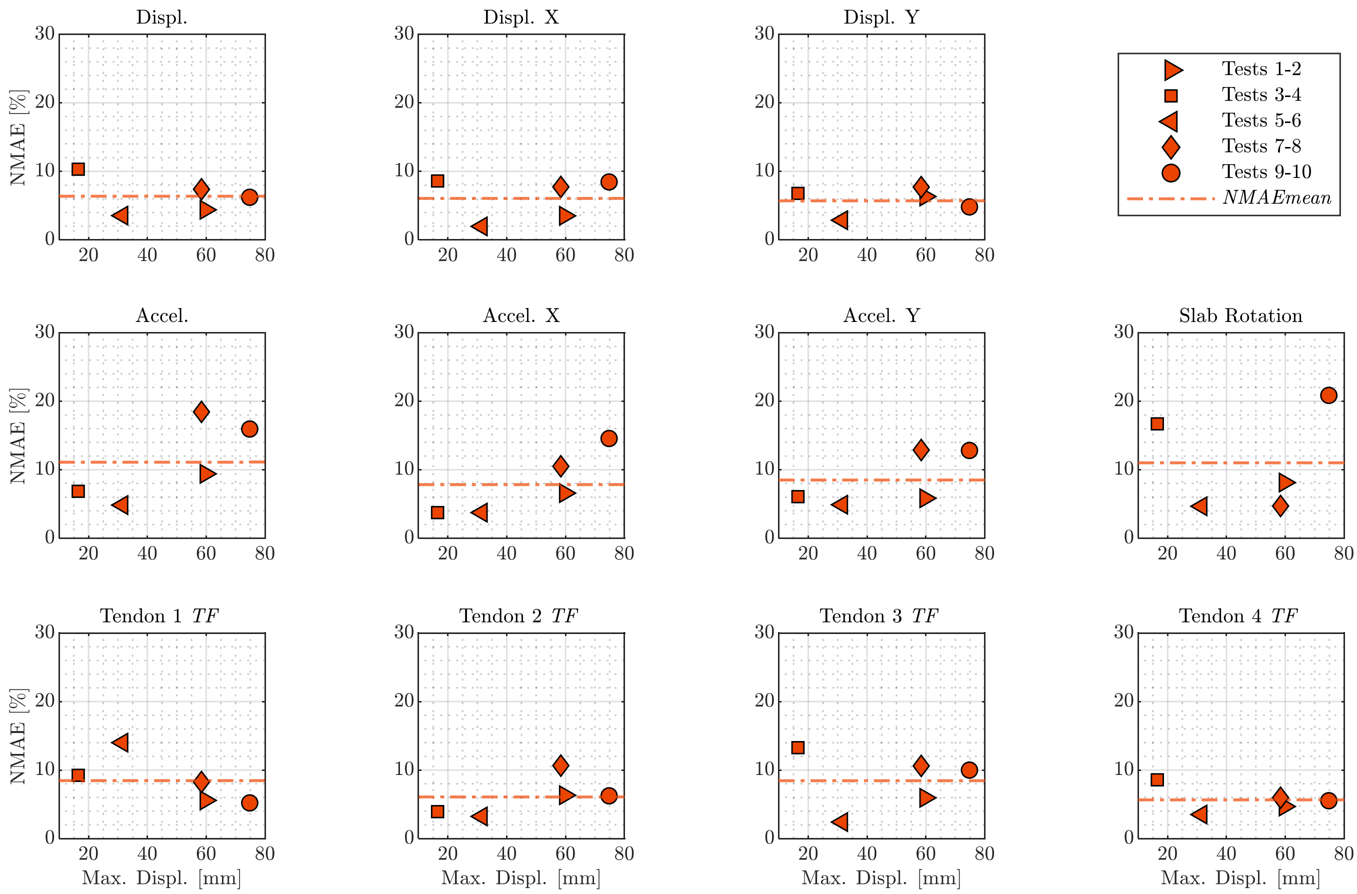

FIGURE 10 | Normalized mean absolute error (NMAE) of the entire time-history.

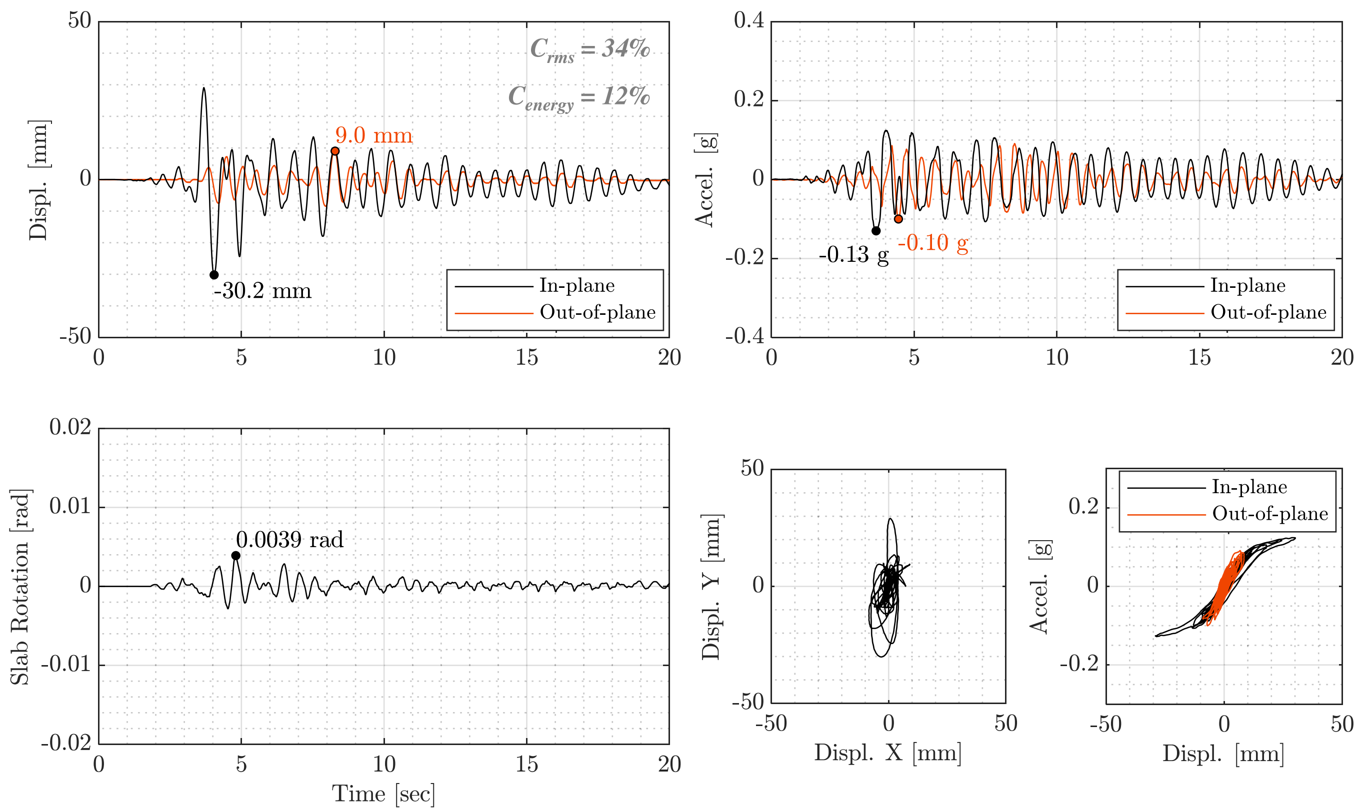

FIGURE 11 | Quantification of the parasitic out-of-plane motion (Test 12).

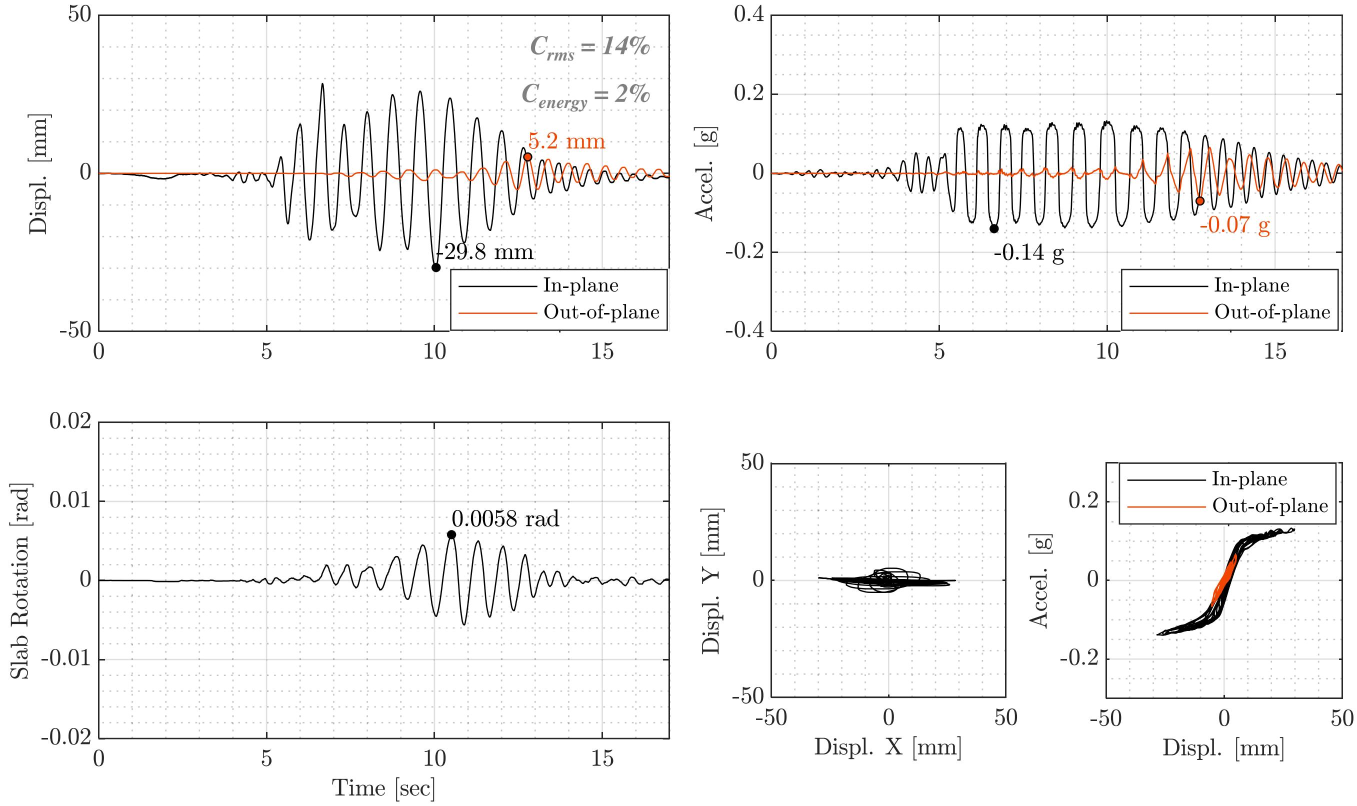

FIGURE 12 | Quantification of the parasitic out-of-plane motion (Test 14).

- Even though the out-of-plane response remains in the pre-uplift phase, the out-of-plane accelerations are significant. For Tests 12 and 14, the out-of-plane to in-plane maximum acceleration is 0.10 g/0.13 g = 77% and 0.07 g/0.14 g = 50% (Figures 11 and 12, top right).
- The in-plane and out-of-plane displacement time histories show low correlation, with $R = 0.46$ and $R = 0.11$, respectively.
- Under planar loading, the maximum slab rotations are very low: 0.0039 and 0.0058 rad. This points to the possibility that slab rotation is amplified under multidirectional excitations. Even though no solid conclusions can be drawn due to the limited number of planar tests, this is worth further investigation to better understand torsion in rocking structures.
- The RMS ratio (C_{rms}) is low: $C_{rms} = 34\%$ and $C_{rms} = 14\%$. This means that the out-of-plane response is on average 14%–34% of the in-plane response.
- The energy-based coupling index is very low ($C_{energy} = 12\%$ and $C_{energy} = 2\%$), hence the out-of-plane response is only a small fraction of the in-plane response.
- The in-plane motion precedes the out-of-plane by 1–5 s, depending on the test (i.e., there is a time lag between the two, with in-plane motion appearing first). This is reasonable, as the out-of-plane motion is a parasitic quantity induced by the in-plane motion that leads to wobbling of the columns.

Figure 13 assesses the accuracy of performing independent planar analyses for two horizontal directions and combining the results to approximate the bidirectional response. Tests 11 and 12 were subjected to only the *X* and *Y* components of the Coalinga-01 (Parkfield—Fault Zone 14) ground motion, respectively (Table 1), and the results were geometrically combined (Section 3.4). Test 13 was simultaneously subjected to both the *X* and *Y* components of the same ground motion (Table 1). The conclusions from Figure 13 are summarized as follows:

- Applying the two horizontal components of the excitation independently and combining them geometrically provides a reasonable, yet *nonconservative*, estimate of the bidirectional response. This is an important conclusion that holds for controlled rocking structures with positive post-uplift stiffness, post-uplift eigenperiod, and geometries similar to the one tested.
- The planar approximation predicts the maximum response of the bidirectional tests well. The error in maximum displacement and maximum acceleration was less than 5%. The maximum rotation error was 8%. The error in maximum tendon forces ranged between 9% and 26%. In all cases, the planar approximation is nonconservative.
- The planar approximation correlates well with the time history of the displacements and accelerations, with $R = 0.61$, NMAE = 9% and $R = 0.73$, NMAE = 11%, respectively.
- The planar approximation significantly underestimates the bidirectional slab rotation ($R = 0.23$ and NMAE = 10%). As in the conclusions from Figures 11 and 12, bidirectional excitations significantly amplify slab rotations.
- Tendon forces depend on the displacements at the corners of the slab, which depend on slab rotation. As the planar approx-

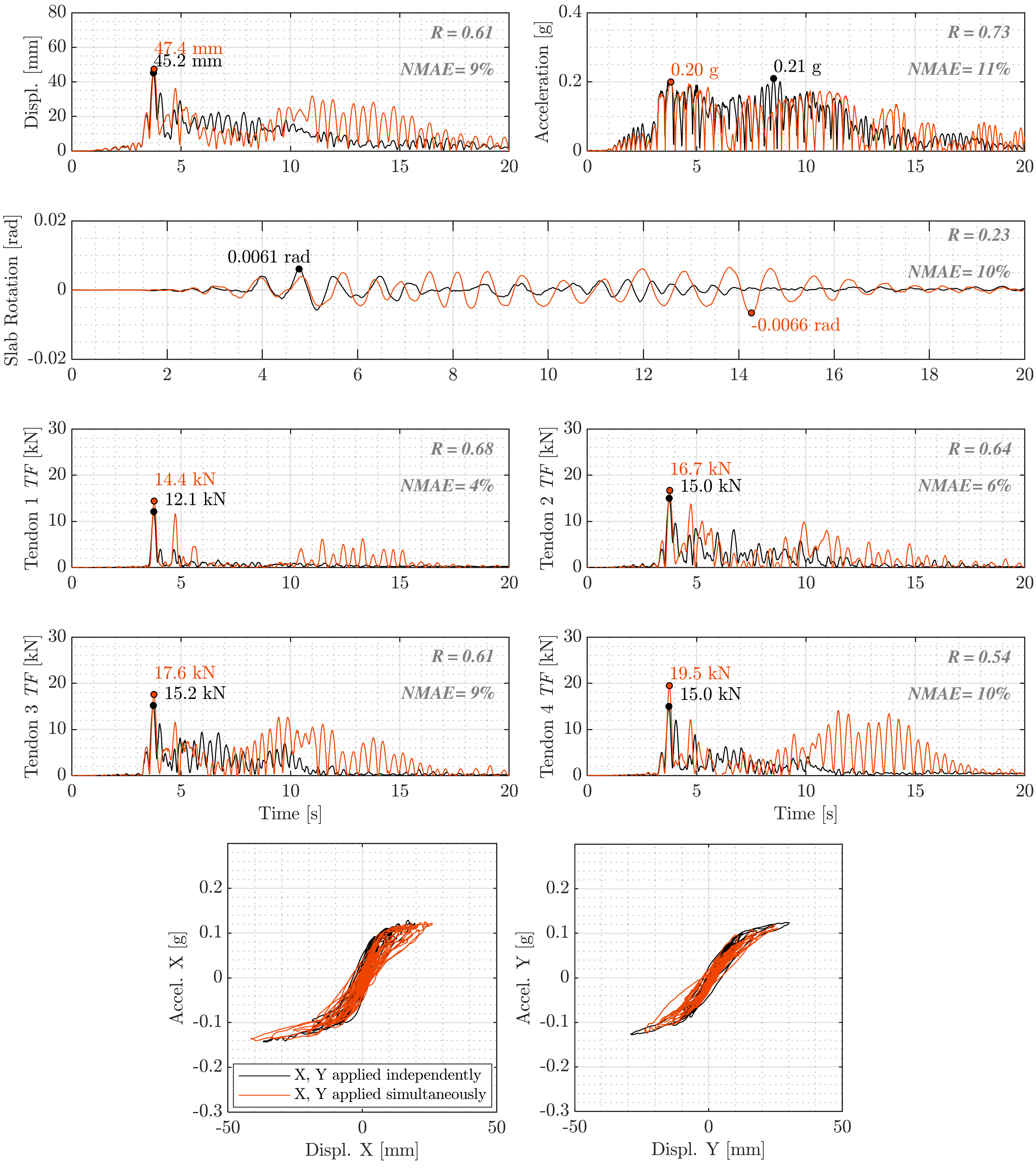

FIGURE 13 | Comparison of the combined response from two planar analyses (Tests 11 and 12) to the bidirectional response (Test 13).

imation underestimates slab rotation, it also underestimates tendon forces, with $R = 0.54$–0.68 and NMAE = 4%–10%.

- The bidirectional test oscillates for a longer time, indicating lower energy dissipation.
- The acceleration–displacement plots match well with negligible differences.

5 | Conclusions

This paper studies the repeatability and the parasitic out-of-plane motion of controlled rocking structures with cylindrical columns through large-scale triaxial shake table tests. Rocking structures outperform conventional ones since they are self-centering and show zero post-earthquake damage. However, their widespread application has been hindered by the perception that rocking is inherently sensitive and unpredictable. This sensitivity is so pronounced in unenhanced rocking that it makes shake table tests nonrepeatable, a phenomenon that led rocking motion to be termed "chaotic."

This study is the first to investigate the repeatability of controlled rocking structures: (i) under large displacements; (ii) with cylindrical columns; (iii) without additional damping; (iv) under triaxial seismic excitation. Moreover, it is the first to investigate the parasitic out-of-plane motion of controlled rocking structures with cylindrical columns. A bridge-like specimen was built and tested under 16 seismic motions in a 1:5 scale. The specimen comprised four slender cylindrical columns capped with a slab. All members were made of reinforced concrete. Unbonded steel tendons were connected at the bottom of the columns and at the top of the slab, leading to a controlled rocking response with positive post-uplift stiffness and a post-uplift eigenperiod of approximately 5 sec. Even though external damping is considered essential to provide repeatable rocking results, the present study did not use auxiliary damping devices; the only damping mechanisms present were those inherent to rocking motion (friction and impact).

While the tests of uncontrolled (unenhanced) rocking structures are nonrepeatable, this study proves that controlled rocking structures with positive post-uplift stiffness are repeatable—even without external damping. The displacement time history was almost perfectly repeatable with average correlation coefficients above 0.85 and errors below 10%. Accelerations and tendon force time histories were slightly more sensitive, yet with high correlation coefficients (around 0.75 and 0.80) and low errors (8% and 10%). Slab rotation around its vertical axis was the only nonrepeatable response magnitude, indicating that rotational kinematics are more sensitive to boundary conditions. Nevertheless, the use of positive translational stiffness kept rotations low and limited their impact on the global response. Most importantly, maximum (peak) responses (which govern design) were highly repeatable with correlation coefficients above 0.9 and errors of 10% for displacements, accelerations, and tendon forces.

When the tested structure was subjected to planar seismic excitations, the observed parasitic out-of-plane motion was limited—in contrast to unenhanced rocking structures. On average, the out-of-plane motion was less than 25% of the in-plane, with peaks at 30%. Since the out-of-plane motion is limited, performing planar tests for each horizontal seismic component and combining them geometrically can provide a reasonable, yet nonconservative, estimate of the bidirectional test. Under planar motion, slab rotations were very low, indicating that bidirectional excitations may amplify torsion.

The findings contradict the perception that controlled rocking is inherently nonrepeatable and that external damping is an absolute necessity. The high repeatability of the response shows that inherent frictional and impact damping can produce repeatable experimental results that can be used for the deterministic assessment of numerical models—at least for designs similar to the one tested. The limited parasitic out-of-plane motion can simplify design and extend the significance of uniaxial shake table tests. The conclusions of the study correspond to a class of structures similar to the one tested (controlled rocking with positive post-uplift stiffness); more tests need to be performed for the full characterization of the described phenomena, including testing at larger scales. Moreover, the development of code-compliant analysis methods for controlled rocking structures would greatly facilitate their applicability in real-world settings.

Acknowledgments

Prof. Michalis Vassiliou and Prof. Charalampos Mouzakis are gratefully acknowledged for designing and executing the tests of Ref. [97] together with the author of this paper.

Data Availability Statement

The data that support the findings of the study are available from the author upon reasonable request.

References

1. C. Zhong and C. Christopoulos, "Self-Centering Seismic-Resistant Structures: Historical Overview and State-of-the-Art," *Earthquake Spectra* 38, no. 2 (2022): 1321–1356, https://doi.org/10.1177/87552930211057581.

2. V. Sarhosis, P. Asteris, T. Wang, W. Hu, and Y. Han, "On the Stability of Colonnade Structural Systems Under Static and Dynamic Loading Conditions," *Bulletin of Earthquake Engineering* 14, no. 4 (2016): 1131–1152, https://doi.org/10.1007/s10518-016-9881-z.

3. D. Konstantinidis and N. Makris, "Seismic Response Analysis of Multidrum Classical Columns," *Earthquake Engineering & Structural Dynamics* 34 (2005): 1243–1270, https://doi.org/10.1002/eqe.478.

4. V. A. Drosos and I. Anastasopoulos, "Experimental Investigation of the Seismic Response of Classical Temple Columns," *Bulletin of Earthquake Engineering* 13, no. 1 (2015): 299–310, https://doi.org/10.1007/s10518-014-9608-y.

5. D. Malomo, M. J. DeJong, and A. Penna, "Distinct Element Modelling of the in-Plane Cyclic Response of URM Walls Subjected to Shear-Compression," *Earthquake Engineering & Structural Dynamics* 48 (2019): 1322–1344, https://doi.org/10.1002/eqe.3178.

6. D. Malomo and M. J. DeJong, "A Macro-Distinct Element Model (M-DEM) for Simulating in-Plane/Out-of-Plane Interaction and Combined Failure Mechanisms of Unreinforced Masonry Structures," *Earthquake Engineering & Structural Dynamics* 51 (2022): 793–811, https://doi.org/10.1002/eqe.3591.

7. A. I. Giouvanidis, E. G. Dimitrakopoulos, and P. B. Lourenço, "Chattering: An Overlooked Peculiarity of Rocking Motion," *Nonlinear Dynamics* 109, no. 2 (2022): 459–477, https://doi.org/10.1007/s11071-022-07578-1.

8. G. Vlachakis, A. I. Giouvanidis, A. Mehrotra, and P. B. Lourenço, "Numerical Block-Based Simulation of Rocking Structures Using a Novel Universal Viscous Damping Model," *Journal of Engineering Mechanics* 147, no. 11 (2021): 04021089, https://doi.org/10.1061/(ASCE)EM.1943-7889.0001985.

9. M. F. Funari, A. Mehrotra, and P. B. Lourenço, "A Tool for the Rapid Seismic Assessment of Historic Masonry Structures Based on Limit Analysis Optimisation and Rocking Dynamics," *Applied Sciences* 11, no. 3 (2021): 942, https://doi.org/10.3390/app11030942.

10. N. Mendes, A. A. Costa, P. B. Lourenço, et al., "Methods and Approaches for Blind Test Predictions of Out-of-Plane Behavior of Masonry Walls: A Numerical Comparative Study," *International Journal of Architectural Heritage* 11, no. 1 (2017): 59–71, https://doi.org/10.1080/15583058.2016.1238974.

11. D. Malomo, R. Pinho, and A. Penna, "Numerical Modelling of the Out-of-Plane Response of Full-Scale Brick Masonry Prototypes Subjected

to Incremental Dynamic Shake-Table Tests," *Engineering Structures* 209 (2020): 110298, https://doi.org/10.1016/j.engstruct.2020.110298.

12. D. Kalliontzis and A. E. Schultz, "Characterizing the in-Plane Rocking Response of Masonry Walls With Unbonded Posttensioning," *Journal of Structural Engineering* 143, no. 9 (2017): 04017110, https://doi.org/10.1061/(ASCE)ST.1943-541X.0001838.

13. M. J. DeJong, "Seismic Response of Stone Masonry Spires: Analytical Modeling," *Engineering Structures* 40 (2012): 556–565, https://doi.org/10.1016/j.engstruct.2012.03.010.

14. F. Graziotti, U. Tomassetti, A. Penna, and G. Magenes, "Out-of-Plane Shaking Table Tests on URM Single Leaf and Cavity Walls," *Engineering Structures* 125 (2016): 455–470, https://doi.org/10.1016/j.engstruct.2016.07.011.

15. U. Tomassetti, F. Graziotti, L. Sorrentino, and A. Penna, "Modelling Rocking Response via Equivalent Viscous Damping," *Earthquake Engineering & Structural Dynamics* 48, no. 11 (2019): 1277–1296, https://doi.org/10.1002/eqe.3182.

16. S. Lagomarsino, "Seismic Assessment of Rocking Masonry Structures," *Bulletin of Earthquake Engineering* 13, no. 1 (2015): 97–128, https://doi.org/10.1007/s10518-014-9609-x.

17. F. Galvez, L. Sorrentino, D. Dizhur, and J. M. Ingham, "Seismic Rocking Simulation of Unreinforced Masonry Parapets and Façades Using the Discrete Element Method," *Earthquake Engineering & Structural Dynamics* 51 (2022): 1840–1856, https://doi.org/10.1002/eqe.3641.

18. L. Giresini, F. Solarino, and O. AlShawa, "Dissipative Tie-Rods Restraining One-Sided Rocking Masonry Walls: Analytical Formulation and Experimental Tests," *Bulletin of Earthquake Engineering* 23, no. 2 (2025): 779–804, https://doi.org/10.1007/s10518-024-02040-6.

19. Y. Bao and D. Konstantinidis, "Dynamics of a Sliding-Rocking Block Considering Impact With an Adjacent Wall," *Earthquake Engineering & Structural Dynamics* 49, no. 5 (2020): 498–523, https://doi.org/10.1002/eqe.3250.

20. T. Das, E. Seylabi, M. Tabbakhhah, and D. McCallen, "Seismic Response of Vertical Dry Storage Casks Under Three-Dimensional Earthquake Motions," *Nuclear Engineering and Design* 444 (2025): 114339, https://doi.org/10.1016/j.nucengdes.2025.114339.

21. A. M. D'Altri, G. Vlachakis, S. de Miranda, and P. B. Lourenço, "Rocking Block Simulation Based on Numerical Dissipation," *Nonlinear Dynamics* 112, no. 20 (2024): 17843–17862.

22. A. A. Katsamakas and M. F. Vassiliou, "Finite Element Analysis of the Dynamic Response of a Free-Standing Cylindrical Column: A Statistical Approach," in *3rd International Conference on Natural Hazards & Infrastructure (ICONHIC2022)* (2022).

23. A. A. Katsamakas and M. F. Vassiliou, "Finite Element Modeling of Free-Standing Cylindrical Columns Under Seismic Excitation," *Earthquake Engineering & Structural Dynamics* 51 (2022): 2016–2035, https://doi.org/10.1002/eqe.3651.

24. P. Liu, Y.-M. Zhang, H.-T. Chen, and W.-G. Yang, "Experimental Study on Rocking Blocks Subjected to Bidirectional Ground and Floor Motions via Shaking Table Tests," *Earthquake Engineering & Structural Dynamics* 52 (2023): 3171–3192, https://doi.org/10.1002/eqe.3918.

25. G. Magliulo, D. D'Angela, and E. Cosenza, "Experimental Assessment of the Seismic Performance of Hospital Cabinets Using Shake Table Testing," *Earthquake Engineering & Structural Dynamics* 48, no. 1 (2019): 103–123.

26. A. Dar, D. Konstantinidis, and W. W. El-Dakhakhni, "Evaluation of ASCE 43-05 Seismic Design Criteria for Rocking Objects in Nuclear Facilities," *Journal of Structural Engineering* 142, no. 11 (2016): 04016110, https://doi.org/10.1061/(ASCE)ST.1943-541X.0001581.

27. D. Konstantinidis and N. Makris, "Experimental and Analytical Studies on the Response of Freestanding Laboratory Equipment to Earthquake Shaking," *Earthquake Engineering & Structural Dynamics* 38 (2009): 827–848, https://doi.org/10.1002/eqe.871.

28. R. Thiers-Moggia and C. Málaga-Chuquitaype, "Seismic Control of Flexible Rocking Structures Using Inerters," *Earthquake Engineering & Structural Dynamics* 49 (2020): 1519–1538, https://doi.org/10.1002/eqe.3315.

29. R. Thiers-Moggia and C. Málaga-Chuquitaype, "Performance-Based Seismic Design and Assessment of Rocking Timber Buildings Equipped With Inerters," *Engineering Structures* 248 (2021): 113164, https://doi.org/10.1016/j.engstruct.2021.113164.

30. S. I. Reyes, J. L. Almazán, M. F. Vassiliou, N. F. Tapia, J. I. Colombo, and J. C. de la Llera, "Full-Scale Shaking Table Test and Numerical Modeling of a 3000-Liter Legged Storage Tank Isolated With a Vertical Rocking Isolation System," *Earthquake Engineering & Structural Dynamics* 51 (2022): 1563–1585, https://doi.org/10.1002/eqe.3628.

31. A. I. Giouvanidis and E. G. Dimitrakopoulos, "Nonsmooth Dynamic Analysis of Sticking Impacts in Rocking Structures," *Bulletin of Earthquake Engineering* 15, no. 5 (2017): 2273–2304, https://doi.org/10.1007/s10518-016-0068-4.

32. G. Destro Bisol, M. J. DeJong, D. Liberatore, and L. Sorrentino, "Displacement-Based Design Procedures for Rigid Block Isolation," *Earthquake Engineering & Structural Dynamics* 53 (2024): 1552–1572, https://doi.org/10.1002/eqe.4074.

33. H. Zhu, M. N. Chatzis, and S. Acikgoz, "A New Model for the Sliding Flexible Rocking Oscillator," *Earthquake Engineering & Structural Dynamics* 54 (2025): 2882–2899, https://doi.org/10.1002/eqe.70006.

34. N. Makris and D. Konstantinidis, "The Rocking Spectrum and the Limitations of Practical Design Methodologies," *Earthquake Engineering & Structural Dynamics* 32 (2003): 265–289, https://doi.org/10.1002/eqe.223.

35. R. Tremblay, L.-P. Poirier, and N. Bouaanani, "Innovative Viscously Damped Rocking Braced Steel Frames," in *14th World Conference on Earthquake Engineering WCEE* (2008).

36. J. Yang, Z. Q. Yang, Y. Chen, Y. Lv, and N. Chouw, "Finite Element Simulation of an Upliftable Rigid Frame Bridge Under Earthquakes: Experimental Verification," *Soil Dynamics and Earthquake Engineering* 165 (2023): 107716, https://doi.org/10.1016/j.soildyn.2022.107716.

37. J. A. Bachmann, M. F. Vassiliou, and B. Stojadinovic, "Rolling and Rocking of Rigid Uplifting Structures," *Earthquake Engineering & Structural Dynamics* 48 (2019): 1556–1574, https://doi.org/10.1002/eqe.3213.

38. N. Makris and M. F. Vassiliou, "Planar Rocking Response and Stability Analysis of an Array of Free-Standing Columns Capped With a Freely Supported Rigid Beam," *Earthquake Engineering & Structural Dynamics* 42 (2013): 431–449, https://doi.org/10.1002/eqe.2222.

39. E. G. Dimitrakopoulos and A. I. Giouvanidis, "Seismic Response Analysis of the Planar Rocking Frame," *Journal of Engineering Mechanics* 141, no. 7 (2015): 04015003, https://doi.org/10.1061/(ASCE)EM.1943-7889.0000939.

40. N. Makris and M. F. Vassiliou, "Dynamics of the Rocking Frame With Vertical Restrainers," *Journal of Structural Engineering* 141 (2015): 04014245, (ASCE)ST.1943-541X.0001231.

41. A. I. Giouvanidis and E. G. Dimitrakopoulos, "Seismic Performance of Rocking Frames With Flag-Shaped Hysteretic Behavior," *Journal of Engineering Mechanics* 143, no. 5 (2017): 04017008, https://doi.org/10.1061/(ASCE)EM.1943-7889.0001206.

42. M. F. Vassiliou and N. Makris, "Dynamics of the Vertically Restrained Rocking Column," *Journal of Engineering Mechanics* 141 (2015): 04015049, EM.1943-7889.0000953 .

43. A. I. Giouvanidis and Y. Dong, "Seismic Loss and Resilience Assessment of Single-Column Rocking Bridges," *Bulletin of Earthquake Engineering* 18 (2020): 4481–4513, https://doi.org/10.1007/s10518-020-00865-5.

44. M. Salehi, P. Sideris, and A. B. Liel, "Experimental Testing of Hybrid Sliding-Rocking Bridge Columns Under Torsional and Biaxial Lateral

Loading," *Earthquake Engineering & Structural Dynamics* 50 (2021): 2817–2837, https://doi.org/10.1002/eqe.3474.

45. A. A. Katsamakas and M. F. Vassiliou, "Finite Element Modeling of the Shake-Table Response of a Bridge-Like Model Comprising Rocking Columns," in *COMPDYN 2023* (2023), https://doi.org/10.7712/120123.10386.20737.

46. A. Katsamakas and M. F. Vassiliou, "Finite Element Modeling of the Seismic Response of a Bridge-Like Model With Restrained Rocking Piers," in *18th World Conference on Earthquake Engineer*ing (WCEE 2024) (2024).

47. M. Mashal and A. Palermo, "Low-Damage Seismic Design for Accelerated Bridge Construction," *Journal of Bridge Engineering* 24 (2019): 04019066, https://doi.org/10.1061/(ASCE)BE.1943-5592.0001406.

48. D. Marriott, S. Pampanin, and A. Palermo, "Biaxial Testing of Unbonded Post-Tensioned Rocking Bridge Piers With External Replacable Dissipaters," *Earthquake Engineering & Structural Dynamics* 40 (2011): 1723–1741, https://doi.org/10.1002/eqe.1112.

49. A. Katsamakas, M. F. Vassiliou, and C. Mouzakis, "Triaxial Shake Table Testing and Finite Element Modeling of a Modular Prefabricated Bridge-Like Specimen With Restrained Rocking Piers," in *19th World Conference on Seismic Isolation (19WCSI)* (2025).

50. S. Piras, A. Palermo, and G. Chiaro, "Numerical Modelling Approaches for Predicting the Seismic Response of Monopole-Supported Dissipative Controlled Rocking Bridge Piers," *Bulletin of the New Zealand Society for Earthquake Engineering* 56, no. 3 (2023): 152–168, https://doi.org/10.5459/bnzsee.1591.

51. Z. Jia, J. Wen, M. Hu, Q. Han, and K. Bi, "Seismic Response of Rocking Bridge Systems Under Three-Dimensional Ground Motions," *Engineering Structures* 322 (2025): 119162, https://doi.org/10.1016/j.engstruct.2024.119162.

52. K. E. Bantilas, I. E. Kavvadias, L. K. Vasiliadis, and A. Elenas, "Seismic Fragility and Intensity Measure Investigation for Rocking Podium Structures Under Synthetic Pulse-Like Excitations," *Earthquake Engineering & Structural Dynamics* 50, no. 13 (2021): 3441–3459, https://doi.org/10.1002/eqe.3517.

53. J. A. Bachmann, M. F. Vassiliou, and B. Stojadinović, "Dynamics of Rocking Podium Structures," *Earthquake Engineering & Structural Dynamics* 46 (2017): 2499–2517, https://doi.org/10.1002/eqe.2915.

54. N. Buccella, L. Wiebe, D. Konstantinidis, and T. Steele, "Demands on Nonstructural Components in Buildings With Controlled Rocking Braced Frames," *Earthquake Engineering & Structural Dynamics* 50, no. 4 (2021): 1063–1082, https://doi.org/10.1002/eqe.3385.

55. T. C. Steele and L. D. Wiebe, "Dynamic and Equivalent Static Procedures for Capacity Design of Controlled Rocking Steel Braced Frames," *Earthquake Engineering & Structural Dynamics* 45, no. 14 (2016): 2349–2369, https://doi.org/10.1002/eqe.2765.

56. Y. Zhang, G. A. MacRae, G. W. Rodgers, et al., "Shaking Table Behaviour of a Full-Scale Three Storey Steel Rocking Structure With Tension-Only Frictional Dissipators," *Earthquake Engineering & Structural Dynamics* 55 (2026): 1769–1787, https://doi.org/10.1002/eqe.70132.

57. F. Freddi, C. A. Dimopoulos, and T. L. Karavasilis, "Rocking Damage-Free Steel Column Base With Friction Devices: Design Procedure and Numerical Evaluation," *Earthquake Engineering & Structural Dynamics* 46, no. 14 (2017): 2281–2300, https://doi.org/10.1002/eqe.2904.

58. F. Freddi, C. A. Dimopoulos, and T. L. Karavasilis, "Experimental Evaluation of a Rocking Damage-Free Steel Column Base With Friction Devices," *Journal of Structural Engineering* 146, no. 10 (2020): 04020217, https://doi.org/10.1061/(ASCE)ST.1943-541X.0002779.

59. A. Lettieri, F. Freddi, and M. Latour, "Experimental Response of Damage-Free Self-Centering Links for Seismic Resilient Eccentrically Braced Frames," *Journal of Structural Engineering* 151, no. 11 (2025): 04025173, https://doi.org/10.1061/JSENDH.STENG-14660.

60. D. S. Pilon, A. Palermo, F. Sarti, and A. Salenikovich, "Benefits of Multiple Rocking Segments for CLT and LVL Pres-Lam Wall Systems," *Soil Dynamics and Earthquake Engineering* 117 (2019): 234–244, https://doi.org/10.1016/j.soildyn.2018.11.026.

61. S. Acikgoz, Q. Ma, A. Palermo, and M. J. DeJong, "Experimental Identification of the Dynamic Characteristics of a Flexible Rocking Structure," *Journal of Earthquake Engineering* 20, no. 8 (2016): 1199–1221, https://doi.org/10.1080/13632469.2016.1138169.

62. B. Wang, S. Zhu, K. Chen, C. X. Qiu, and P. Chen, "Damage-Free Self-Centering Steel Columns Incorporating SMA Bolts and Replaceable Steel Angles," *Engineering Structures* 321 (2024): 119000, https://doi.org/10.1016/j.engstruct.2024.119000.

63. S. Hu, S. Zhu, W. Wang, and M. S. Alam, "Structural and Nonstructural Damage Assessment of Steel Buildings Equipped With Self-Centering Energy-Absorbing Rocking Core Systems: A Comparative Study," *Journal of Constructional Steel Research* 198 (2022): 107559, https://doi.org/10.1016/j.jcsr.2022.107559.

64. M. A. Kovacs and L. Wiebe, "Controlled Rocking CLT Walls for Buildings in Regions of Moderate Seismicity: Design Procedure and Numerical Collapse Assessment," *Journal of Earthquake Engineering* 23, no. 5 (2019): 750–770, https://doi.org/10.1080/13632469.2017.1326421.

65. T. C. Steele and L. D. Wiebe, "Collapse Risk of Controlled Rocking Steel Braced Frames With Different Post-Tensioning and Energy Dissipation Designs," *Earthquake Engineering & Structural Dynamics* 46, no. 13 (2017): 2063–2082, https://doi.org/10.1002/eqe.2892.

66. C. Christopoulos, R. Tremblay, H. J. Kim, and M. Lacerte, "Self-Centering Energy Dissipative Bracing System for the Seismic Resistance of Structures: Development and Validation," *Journal of structural engineering* 134, no. 1 (2008): 96–107, https://doi.org/10.1061/(ASCE)0733-9445(2008)134:1(96).

67. R. Tremblay, M. Lacerte, and C. Christopoulos, "Seismic Response of Multistory Buildings With Self-centering Energy Dissipative Steel Braces," *Journal of Structural Engineering* 134, no. 1 (2008): 108–120, https://doi.org/10.1061/(ASCE)0733-9445(2008)134:1(108.

68. J. Erochko, C. Christopoulos, R. Tremblay, and H. J. Kim, "Shake Table Testing and Numerical Simulation of a Self-Centering Energy Dissipative Braced Frame," *Earthquake Engineering & Structural Dynamics* 42, no. 11 (2013): 1617–1635, https://doi.org/10.1002/eqe.2290.

69. N. Makris, "A Half-Century of Rocking Isolation," *Earthquakes and Structures* 7, no. 6 (2014): 1187–1221, https://doi.org/10.12989/eas.2014.7.6.1187.

70. C. S. Yim, A. K. Chopra, and J. Penzien, "Rocking Response of Rigid Blocks to Earthquakes," *Earthquake Engineering & Structural Dynamics* 8 (1980): 565–587, https://doi.org/10.1002/eqe.4290080606.

71. S. C. Yim and H. Lin, "Nonlinear Impact and Chaotic Response of Slender Rocking Objects," *Journal of Engineering Mechanics* 117, no. 9 (1991): 2079–2100, https://doi.org/10.1061/(ASCE)0733-9399(1991)117:9(2079).

72. M. Aslam, W. G. Godden, and D. T. Scalise, "Earthquake Rocking Response of Rigid Bodies," *Journal of the Structural Division* 106, no. 2 (1980): 377–392, https://doi.org/10.1061/JSDEAG.0005363.

73. C. G. Lachanas and D. Vamvatsikos, "Rocking Incremental Dynamic Analysis," *Earthquake Engineering & Structural Dynamics* 51, no. 3 (2022): 688–703, https://doi.org/10.1002/eqe.3586.

74. C. G. Lachanas, D. Vamvatsikos, and M. F. Vassiliou, "The Influence of the Vertical Component of Ground Motion on the Probabilistic Treatment of the Rocking Response of Free-Standing Blocks," *Earthquake Engineering & Structural Dynamics* 51, no. 8 (2022): 1874–1894, https://doi.org/10.1002/eqe.3643.

75. V. Drosos and I. Anastasopoulos, "Shaking Table Testing of Multidrum Columns and Portals," *Earthquake Engineering & Structural Dynamics* 43 (2014): 1703–1723, https://doi.org/10.1002/eqe.2418.

76. M. F. Vassiliou, C. Cengiz, M. Dietz, et al., "Data Set From Shake Table Tests of Free-Standing Rocking Bodies," *Earthquake Spectra* 37, no. 4 (2021): 2971–2987, https://doi.org/10.1177/87552930211020021.

77. M. F. Vassiliou, M. Broccardo, C. Cengiz, et al., "Shake Table Testing of a Rocking Podium: Results of a Blind Prediction Contest," *Earthquake Engineering & Structural Dynamics* 50 (2021): 1043–1062, https://doi.org/10.1002/eqe.3386.

78. D. Malomo, A. Mehrotra, and M. J. DeJong, "Distinct Element Modeling of the Dynamic Response of a Rocking Podium Tested on a Shake Table," *Earthquake Engineering & Structural Dynamics* 50 (2021): 1469–1475, https://doi.org/10.1002/eqe.3404.

79. C. Zhong and C. Christopoulos, "Finite Element Analysis of the Seismic Shake-Table Response of a Rocking Podium Structure," *Earthquake Engineering & Structural Dynamics* 50 (2021): 1223–1230, https://doi.org/10.1002/eqe.3397.

80. C. Zhong and C. Christopoulos, "Shear-Controlling Rocking-Isolation Podium System for Enhanced Resilience of High-Rise Buildings," *Earthquake Engineering & Structural Dynamics* 51 (2022): 1363–1382, https://doi.org/10.1002/eqe.3619.

81. C. Zhong and C. Christopoulos, "Scaled Shaking Table Testing of Higher-Mode Effects on the Seismic Response of Tall and Slender Structures," *Earthquake Engineering & Structural Dynamics* 52 (2023): 549–570, https://doi.org/10.1002/eqe.3772.

82. C. Zhong and C. Christopoulos, "Seismic Response of Slender MDOF Structures With Self-Centering Base Shear and Moment Mechanisms," *Earthquake Engineering & Structural Dynamics* 52 (2023): 1658–1677, https://doi.org/10.1002/eqe.3834.

83. L. Del Giudice, R. Wrobel, A. A. Katsamakas, C. Leinenbach, and M. F. Vassiliou, "Physical Modelling of Reinforced Concrete at a 1:40 Scale Using Additively Manufactured Reinforcement Cages," *Earthquake Engineering & Structural Dynamics* 51 (2022): 537–551.

84. L. Del Giudice, A. Katsamakas, B. Liu, V. Sarhosis, and M. F. Vassiliou, "Physical Modelling of Unreinforced Masonry Walls Using a Sand-Based 3D Printer," *Engineering Structures* 305 (2024): 117665.

85. J. A. Bachmann, M. Strand, M. F. Vassiliou, M. Broccardo, and B. Stojadinović, "Is Rocking Motion Predictable?," *Earthquake Engineering & Structural Dynamics* 47, no. 2 (2018): 535–552, https://doi.org/10.1002/eqe.2978.

86. A. A. Katsamakas and M. F. Vassiliou, "Experimental Parametric Study and Phenomenological Modeling of a Deformable Rolling Seismic Isolator," *Journal of Earthquake Engineering* 27 (2023): 4664–4693, https://doi.org/10.1080/13632469.2023.2189978.

87. M. Elmorsy, L. Jones, M. Wild, et al., "Benchmark Dataset From Centrifuge Shake Table Tests of 3D-Printed Unreinforced Masonry Structures for Seismic Model Validation," *Earthquake Spectra* 42, no. 1 (2026): e70042, https://doi.org/10.1002/esp4.70042.

88. L. Del Giudice, R. Wrobel, A. A. Katsamakas, C. Leinenbach, and M. F. Vassiliou, "Cyclic Testing of 1: 40 Scale Cantilever RC Elements With Digitally Manufactured Reinforcement," in COMPDYN 2021: Computational Methods in Structural Dynamics and Earthquake Engineering, vol. 1 (2021), 1053–1062.

89. M. Zaki, C. Zhong, and C. Christopoulos, "Analytical Study on the Predictability of Controlled Rocking Frame and Podium Systems," *Earthquake Engineering & Structural Dynamics* 54 (2025): 1558–1578, https://doi.org/10.1002/eqe.4323.

90. M. Midorikawa, T. Azuhata, T. Ishihara, and A. Wada, "Shaking Table Tests on Seismic Response of Steel Braced Frames With Column Uplift," *Earthquake Engineering & Structural Dynamics* 35, no. 14 (2006): 1767–1785, https://doi.org/10.1002/eqe.603.

91. P. Mottier, R. Tremblay, and C. Rogers, "Shake Table Test of a Two-Story Steel Building Seismically Retrofitted Using Gravity-Controlled Rocking Braced Frame System," *Earthquake Engineering & Structural Dynamics* 50, no. 6 (2021): 1576–1594, https://doi.org/10.1002/eqe.3411.

92. L. Wiebe and C. Christopoulos, "Mitigation of Higher Mode Effects in Base-Rocking Systems by Using Multiple Rocking Sections," *Journal of Earthquake Engineering* 13, no. S1 (2009): 83–108, https://doi.org/10.1080/13632460902813315.

93. L. Wiebe and C. Christopoulos, "Performance-Based Seismic Design of Controlled Rocking Steel Braced Frames. I: Methodological Framework and Design of Base Rocking Joint," *Journal of Structural Engineering* 141, no. 9 (2015): 04014226, https://doi.org/10.1061/(ASCE)ST.1943-541X.0001202.

94. L. Wiebe and C. Christopoulos, "Performance-Based Seismic Design of Controlled Rocking Steel Braced Frames. II: Design of Capacity-Protected Elements," *Journal of Structural Engineering* 141, no. 9 (2015): 04014227, https://doi.org/10.1061/(ASCE)ST.1943-541X.0001201.

95. L. Wiebe, C. Christopoulos, R. Tremblay, and M. Leclerc, "Mechanisms to Limit Higher Mode Effects in a Controlled Rocking Steel Frame. 1: Concept, Modelling, and Low-Amplitude Shake Table Testing," *Earthquake Engineering & Structural Dynamics* 42, no. 7 (2013): 1053–1068, https://doi.org/10.1002/eqe.2259.

96. L. Wiebe, C. Christopoulos, R. Tremblay, and M. Leclerc, "Mechanisms to Limit Higher Mode Effects in a Controlled Rocking Steel Frame. 2: Large-Amplitude Shake Table Testing," *Earthquake Engineering & Structural Dynamics* 42, no. 7 (2013): 1069–1086, https://doi.org/10.1002/eqe.2258.

97. A. A. Katsamakas, M. F. Vassiliou, and C. Mouzakis, "Shake Table Testing and Finite Element Modeling of a Modular Prefabricated Concrete Bridge-Like Specimen Accounting for Geometry Imperfections and Additional Damping," *Earthquake Engineering & Structural Dynamics* 53 (2024): 3607–3629, https://doi.org/10.1002/eqe.4189.

98. N. Reggiani Manzo and M. F. Vassiliou, "Cyclic Tests of a Precast Restrained Rocking System for Sustainable and Resilient Seismic Design of Bridges," *Engineering Structures* 252 (2022): 113620, https://doi.org/10.1016/j.engstruct.2021.113620.

99. N. Reggiani Manzo, M. F. Vassiliou, H. Mouzakis, and E. Badogiannis, "Shaking Table Tests of a Resilient Bridge System With Precast Reinforced Concrete Columns Equipped With Springs," *Earthquake Engineering & Structural Dynamics* 51 (2022): 213–239, https://doi.org/10.1002/eqe.3563.

100. A. A. Katsamakas, G. Belser, M. F. Vassiliou, and M. Blondet, "Experimental Investigation of a Spherical Rubber Isolator for Use in Low Income Countries," *Engineering Structures* 250 (2022): 113522, https://doi.org/10.1016/j.engstruct.2021.113522.

101. N. Reggiani Manzo, M. F. Vassiliou, H. Mouzakis, E. Badogiannis, and L. Karapitta, "Development of a Dataset from Shaking Table Tests of a Bridge System With Precast Reinforced Concrete Columns Equipped With Springs," *Journal of Structural Engineering* 148, no. 11 (2022): 04722003.

102. FEMA P695, *Quantification of Building Seismic Performance Factors* (Federal Emergency Management Agency, 2009).

103. European Committee for Standardization (CEN), *Eurocode 8: Design of Structures for Earthquake Resistance, Part 1: General Rules, Seismic Actions and Rules for Buildings*, EN 1998-1:2004 (2004).

104. J. E. Luco, O. Ozcelik, and J. P. Conte, "Acceleration Tracking Performance of the UCSD-NEES Shake Table," *Journal of Structural Engineering* 136, no. 5 (2010): 481–490, https://doi.org/10.1061/(ASCE)ST.1943-541X.0000137.

105. L. Wasserman, *All of Statistics: A Concise Course in Statistical Inference* (Springer Science & Business Media, 2004).